

On the Interference between Meson Exchange and One-Body Currents in Quasielastic Electron Scattering

P.R. Casale,^{1,2,*} J.E. Amaro,^{1,2,†} V. Belocchi,^{3,4,5} M.B. Barbaro,^{3,4} A De Pace,⁴ and M. Martini^{6,7}

¹*Departamento de Física Atómica, Molecular y Nuclear*

²*Instituto Carlos I de Física Teórica y Computacional Universidad de Granada, E-18071 Granada, Spain.*

³*Dipartimento di Fisica Università di Torino, P. Giuria 1, 10125 Torino, Italy*

⁴*INFN Sezione di Torino, 10125 Torino, Italy*

⁵*Instituto de Física Corpuscular (IFIC), Consejo Superior de Investigaciones Científicas (CSIC) and Universidad de Valencia, E-46980 Paterna, Valencia, Spain*

⁶*IPSA-DRII, 63 boulevard de Brandebourg, 94200 Ivry-sur-Seine, France*

⁷*Sorbonne Université, CNRS/IN2P3,*

Laboratoire de Physique Nucléaire et de Hautes Energies (LPNHE), 75005 Paris, France

(Dated: March 12, 2025)

In this work, we present a detailed analysis of the interference between meson exchange currents (MEC) and one-body currents in quasielastic electron scattering, with a focus on the sign of this interference in the transverse response for one-particle emission. We prove that the interference of both the Delta and pion-in-flight currents with the one-body current is negative, leading to a partial cancellation with the seagull current. This is mathematically demonstrated within the framework of the Fermi gas model. By comparing these interferences across various independent particle models, both relativistic and non-relativistic, our results indicate that all studied models display the same behavior. This consistency suggests that the interference is negative in models that do not incorporate tensor correlations in the nuclear wave function.

I. INTRODUCTION

Quasielastic electron scattering plays a pivotal role in probing nuclear structure and dynamics [1, 2]. This scattering process, wherein an electron scatters off a nucleon causing it to be ejected from the nucleus, provides a wealth of information about the underlying nuclear response functions. These response functions provide insight into the distribution of charges and currents in the nucleus and the dynamics of nucleons within the nuclear medium [3–10].

The analysis of current accelerator-based neutrino experiments necessitates a thorough understanding of the probability of neutrino interactions with nuclei [11–19]. Given the challenges in obtaining precise measurements of neutrino-nucleus cross-sections, nuclear models of reactions, such as the (ν_μ, μ^-) charge-changing processes, are indispensable. Neutrino-induced reactions are closely related to electron-induced reactions; in both cases, the electroweak current is explored —within the weak sector for neutrinos and the electromagnetic sector for electrons. Therefore, the same nuclear models used to describe electron scattering can, in principle, be extended to the case of neutrino scattering by modifying the nuclear current operator. A significant contribution to (ν_μ, μ^-) process arises from the quasielastic region, dominated by single-particle emission, although the importance of two-particle emission has also been recognized. In this study, we focus on the single-particle emission, excluding pion

production and inelastic processes.

Analyses of electron and neutrino scattering data have indicated the necessity of including mechanisms that enhance the transverse response [20, 21], with meson-exchange currents (MEC) identified as a potential source [10, 22]. MEC, being two-body operators, can induce both single-particle (1p1h) and two-particle (2p2h) excitations within independent particle models (Fermi gas, Mean field). The specific 2p2h channel has been extensively studied [23–32], demonstrating an important enhancement of the transverse response in the dip region (between the QE and the Δ peaks). While discrepancies exist among various approaches, there is a consensus that 2p2h emission can enhance the inclusive CCQE neutrino cross section about 15 to 20%, thus achieving better agreement with experimental data when these effects are considered alongside pion emission.

The effect of MEC in the 1p1h channel, where one-body (1b) currents interfere with two-body (2b) currents [33–35], has received less attention in the modeling of neutrino scattering and is more controversial. Independent particle models (IPM) —Fermi gas, mean field— typically predict a small and negative MEC effect due to a cancellation between the positive seagull and negative pion-in-flight (or pionic) and Δ currents in the transverse response. At intermediate momentum transfers ($q \sim 500 \text{ MeV}/c$), the Δ current dominates, leading to a small reduction in the transverse response. This reduction arises because, in the matrix element of the MEC between the ground state and a 1p1h excitation, the direct term is negligible or zero, with the exchange term causing a net reduction [36–41].

In contrast, calculations by Fabrocini [42] in nuclear matter within the correlated basis function (CBF) the-

*Electronic address: palomacasale@ugr.es

†Electronic address: amaro@ugr.es

ory have shown a positive effect on the transverse response. This positive effect was identified as due to tensor correlations between nucleons [10, 43]. When these correlations are omitted in Fabrocini’s calculations, the results align with those of independent particle models. The MEC effect in CBF results also agree with Green’s function Monte Carlo (GFMC) calculations by Carlson et al. [10, 44], which include an accurate representation of the wave function, incorporating short-range correlations, and showing an enhancement of the transverse response. This agreement extends to calculations in light nuclei [10]. However, in the context of GFMC and *ab-initio* calculations, as well as in light nuclei, it is generally not possible to separate the one-particle from two-particle emission channels. In these approaches, the calculations typically rely on expected values of operators over the ground state, with no direct information on the final states being obtained. This limits the ability to distinctly resolve contributions from different emission channels.

One of the motivations for the present work is that some recent calculations using independent-particle [45, 46] or spectral function [47] models have reported a large and positive interference of one-body and two-body currents in the transverse response, without the need for tensor correlations in the nuclear wave function. These results contradict previous calculations mentioned earlier, and their origin is not entirely understood, necessitating further clarification. A detailed study, such as the one presented in this article, is required to systematically analyze the theoretical foundations of the interference response and to assess whether the observed discrepancies arise from fundamental differences in the modeling of nuclear dynamics or from specific approximations used in these calculations.

To that end in this article we demonstrate in detail two theorems for low momentum transfer. The low momentum theorems will help shed light on this matter, as models based on similar assumptions should approximately coincide under non-relativistic conditions for low momentum transfer. Specifically, we will show that the interference of the Δ current with the one-body current in the transverse response is negative within the non-relativistic Fermi gas model. Similarly, the interference of the pion-in-flight current with the one-body current is also negative, leading to a partial cancellation with the positive interference of the seagull current. We will demonstrate the theorems in detail, including all relevant formulas and, where applicable, analytical results, ensuring that our calculations with the Fermi gas will be reproducible. This is scientifically desirable to avoid any reasonable doubt.

We will then show, through calculations using a series of independent particle models (IPM), including relativistic Fermi gas (RFG) mean field, plane wave approximation, spectral function, relativistic mean field, and Dirac-equation based shell model, that all of them yield similar results for the 1b2b interference transverse re-

sponse. This demonstrates that all these models without tensor correlations do not violate the theorems for low to intermediate values of the momentum transfer.

We proceed systematically in Section II introducing the formalism of electron scattering, starting with the relativistic MEC model of ref. [41]. By taking the non-relativistic limit, we first obtain the MEC expressions for low energy-momentum, verifying that we arrive at the non-relativistic Riska’s expressions [48], which are the standard operators typically used in calculations including the seagull, pion-in-flight, and Delta currents [50–52].

At the end of Section II we demonstrate two low momentum theorems that establish the negative interference of the Δ and pion-in-flight currents with the one-body current. We compute in detail the 1p1h matrix element of the non-relativistic MEC between plane waves, providing analytical expressions after performing explicitly the spin sums. Furthermore, we will derive the formulas for the one-body–two-body (1b2b) interferences, explicitly demonstrating that the pion-in-flight and Delta contributions are negative.

In the results Section III we will compare the interference responses calculated with various independent particle models (IPM). Specifically, we will consider the relativistic and non-relativistic Fermi gas models, the relativistic mean field of nuclear matter, the mean field with Woods-Saxon potential, the Dirac equation-based potential, and the plane wave approximation (PWA), illustrating the similarities and differences in the OB-MEC transverse interference response. Additionally, we will examine the superscaling model and the spectral function model. Finally, in Section IV, we will present our conclusions.

II. FORMALISM

In this section, we present the formalism of electron scattering and the current operators, including both one-body and meson exchange currents (MECs). We begin with the relativistic expressions and proceed to the non-relativistic limit, which will be applied in the low momentum transfer kinematics. We maintain a detailed level of discussion, providing many mathematical details that are already known, with the aim of making the content understandable to a high proportion of interested readers who may not be experts in the field. This didactic component is intended to ensure that our results are reproducible by anyone who wishes to do so.

A. Response functions

The starting point is the inclusive electron scattering cross section in plane-wave Born approximation with one photon exchange. The exchanged photon is virtual, carrying an energy transfer ω and a momentum transfer \mathbf{q} to the nucleus. We choose the z -axis in the direction of

\mathbf{q} . The initial electron energy is ϵ , and the final electron exits the interaction region with a scattering angle θ and an energy $\epsilon' = \epsilon - \omega$. As usual, we use units where $\hbar = c = 1$. The double-differential cross section can be written as

$$\frac{d\sigma}{d\Omega d\epsilon'} = \sigma_M \left[\frac{Q^4}{q^4} R_L + \left(\tan^2 \frac{\theta}{2} - \frac{Q^2}{2q^2} \right) R_T \right], \quad (1)$$

where σ_M is the Mott cross section and $Q^2 = \omega^2 - q^2 < 0$ is the square of the four-momentum transfer. The longitudinal and transverse response functions, $R_L(q, \omega)$ and $R_T(q, \omega)$, depend only on $q = |\mathbf{q}|$ and ω , and are defined as the following components of the hadronic tensor

$$R_L(q, \omega) = W^{00}, \quad R_T(q, \omega) = W^{11} + W^{22}. \quad (2)$$

The inclusive hadronic tensor, $W^{\mu\nu}$, is constructed from the matrix elements of the electromagnetic current operator, $\hat{J}^\mu(\mathbf{q})$, between the initial and final hadronic states. In this article, we mainly focus on independent particle models where the ground state is approximated by a Slater determinant of single particle wave functions. In particular, we examine the Fermi gas (FG) model, where the single particle states are plane waves $\psi(\mathbf{r}) = e^{i\mathbf{p}\cdot\mathbf{r}}/\sqrt{V}$, and $V \rightarrow \infty$ is the volume of the system. We only consider the final states that are 1p1h excitations, obtained by promoting a state above the Fermi level. Other contributions to the response, such as those due to multinucleon emission or pion emission, are out of the scope of this work. The 1p1h hadronic tensor in the FG model is

$$W_{1p1h}^{\mu\nu} = \sum_{ph} \langle ph^{-1} | \hat{J}^\mu(\mathbf{q}) | F \rangle^* \langle ph^{-1} | \hat{J}^\nu(\mathbf{q}) | F \rangle \times \delta(E_p - E_h - \omega) \theta(p - k_F) \theta(k_F - h) \quad (3)$$

where $|p\rangle \equiv |\mathbf{p}s_p t_p\rangle$ and $|h\rangle \equiv |\mathbf{h}s_h t_h\rangle$ are plane wave states for particles and holes, respectively, and $|F\rangle$ is the FG ground state with all momenta occupied below the Fermi momentum k_F . The delta function ensures energy conservation in the reaction. In the thermodynamic limit, $V \rightarrow \infty$, the above sums are transformed into integrals:

$$\sum_h \rightarrow V \sum_{s_h t_h} \int \frac{d^3h}{(2\pi)^3}. \quad (4)$$

We expand the electromagnetic current as the sum of one-body (1b) plus two-body (2b) currents

$$\hat{J}^\mu(\mathbf{q}) = \hat{J}_{1b}^\mu(\mathbf{q}) + \hat{J}_{2b}^\mu(\mathbf{q}), \quad (5)$$

Where \hat{J}_{1b} is the usual electromagnetic current of the nucleon, while \hat{J}_{2b} denotes two-body meson-exchange currents (MEC). The matrix element of these operators between the nuclear ground state and a 1p1h excitation are given by

$$\langle ph^{-1} | \hat{J}_{1b}^\mu | F \rangle = \langle p | \hat{J}_{1b}^\mu | h \rangle, \quad (6)$$

$$\langle ph^{-1} | \hat{J}_{2b}^\mu | F \rangle = \sum_{k < k_F} \left[\langle pk | \hat{J}_{2b}^\mu | hk \rangle - \langle pk | \hat{J}_{2b}^\mu | kh \rangle \right]. \quad (7)$$

The antisymmetry of the total A -body wave function implies that the matrix element of the MEC in Eq. (7) is the sum of a direct part minus an exchange part, and there is a sum over spectator states, $k < k_F$, in the Fermi gas, Note that the spectator nucleon, $|k\rangle = |ks_k t_k\rangle$, does not change its state nor receive any excitation energy or momentum.

The elementary matrix elements of the 1b and 2b currents between plane waves states can be written as:

$$\begin{aligned} \langle p | \hat{J}_{1b}^\mu | h \rangle &= \frac{(2\pi)^3}{V} \delta^3(\mathbf{q} + \mathbf{h} - \mathbf{p}) j_{1b}^\mu(\mathbf{p}, \mathbf{h}), \quad (8) \\ \langle p'_1 p'_2 | \hat{J}_{2b}^\mu | p_1 p_2 \rangle &= \frac{(2\pi)^3}{V^2} \delta^3(\mathbf{p}_1 + \mathbf{p}_2 + \mathbf{q} - \mathbf{p}'_1 - \mathbf{p}'_2) \\ &\quad \times j_{2b}^\mu(\mathbf{p}'_1, \mathbf{p}'_2, \mathbf{p}_1, \mathbf{p}_2), \quad (9) \end{aligned}$$

where the Dirac deltas arise from momentum conservation. The current functions $j_{1b}^\mu(\mathbf{p}, \mathbf{h})$ and $j_{2b}^\mu(\mathbf{p}'_1, \mathbf{p}'_2, \mathbf{p}_1, \mathbf{p}_2)$ implicitly depend on spin and isospin indices.

If we define the function

$$j_{2b}^\mu(\mathbf{p}, \mathbf{h}) \equiv \frac{1}{V} \sum_{k < k_F} [j_{2b}^\mu(\mathbf{p}, \mathbf{k}, \mathbf{h}, \mathbf{k}) - j_{2b}^\mu(\mathbf{p}, \mathbf{k}, \mathbf{k}, \mathbf{h})], \quad (10)$$

then the MEC matrix element can be written in the same way as that of a one-body operator:

$$\langle ph^{-1} | \hat{J}_{2b}^\mu | F \rangle = \frac{(2\pi)^3}{V} \delta^3(\mathbf{q} + \mathbf{h} - \mathbf{p}) j_{2b}^\mu(\mathbf{p}, \mathbf{h}). \quad (11)$$

Therefore the transition matrix element of the total current between the ground state and the 1p1h state is

$$\langle ph^{-1} | \hat{J}^\mu | F \rangle = \frac{(2\pi)^3}{V} \delta^3(\mathbf{q} + \mathbf{h} - \mathbf{p}) j^\mu(\mathbf{p}, \mathbf{h}), \quad (12)$$

whith and effective one-body current for the 1p1h excitation

$$j^\mu(\mathbf{p}, \mathbf{h}) = j_{1b}^\mu(\mathbf{p}, \mathbf{h}) + j_{2b}^\mu(\mathbf{p}, \mathbf{h}). \quad (13)$$

By inserting (12) into Eq. (3), taking the thermodynamic limit, and integrating over the particle momentum, \mathbf{p} , using the Dirac delta of momentum, the hadronic tensor of the Fermi gas can be written as

$$\begin{aligned} W^{\mu\nu} &= \frac{V}{(2\pi)^3} \sum_{t_h} \int d^3h \delta(E_p - E_h - \omega) 2w^{\mu\nu}(\mathbf{p}, \mathbf{h}) \\ &\quad \times \theta(p - k_F) \theta(k_F - h), \quad (14) \end{aligned}$$

where $\mathbf{p} = \mathbf{h} + \mathbf{q}$. This is exactly the same formula as with the one-body current, with the difference that the current now includes the contribution of the MEC. The function

$w^{\mu\nu}$ is the effective single-nucleon hadronic tensor in the transition $h \rightarrow p$

$$w^{\mu\nu}(\mathbf{p}, \mathbf{h}) = \frac{1}{2} \sum_{s_p s_h} j^\mu(\mathbf{p}, \mathbf{h})^* j^\nu(\mathbf{p}, \mathbf{h}). \quad (15)$$

This single-nucleon tensor implicitly refers either to a proton or a neutron, and the summation over isospin t_h in Eq. (14) corresponds to summing the responses of protons, $t_h = \frac{1}{2}$, and neutrons, $t_h = -\frac{1}{2}$, together.

The effective single-nucleon tensor incorporates the contribution of the MEC, implying there is interference between 1b and 2b currents. In fact, the response functions only involve diagonal elements of the hadronic tensor, and the transverse component $\mu\mu$ (with $\mu = 1, 2$) can be expanded as

$$\begin{aligned} w^{\mu\mu}(\mathbf{p}, \mathbf{h}) &= \frac{1}{2} \sum_{s_p s_h} |j_{1b}^\mu(\mathbf{p}, \mathbf{h}) + j_{2b}^\mu(\mathbf{p}, \mathbf{h})|^2 \\ &= w_{1b}^{\mu\mu} + w_{1b2b}^{\mu\mu} + w_{2b}^{\mu\mu}, \end{aligned} \quad (16)$$

where

$$w_{1b}^{\mu\mu} = \frac{1}{2} \sum |j_{1b}^\mu|^2, \quad (17)$$

$$w_{1b2b}^{\mu\mu} = \text{Re} \sum (j_{1b}^\mu)^* j_{2b}^\mu, \quad (18)$$

$$w_{2b}^{\mu\mu} = \frac{1}{2} \sum |j_{2b}^\mu|^2. \quad (19)$$

The first term, $w_{1b}^{\mu\mu}$, is the tensor corresponding to the one-body current alone, $w_{1b2b}^{\mu\mu}$ is the interference between 1b and 2b currents, and $w_{2b}^{\mu\mu}$ represents the contribution of the two-body current alone. The 1b part is the leading contribution in the quasielastic peak, while the dominant contribution of the MEC corresponds to the interference with the one-body current [38, 40], being the pure contribution of the two-body current generally smaller.

Therefore the transverse response function is the sum of a response induced by the one-body current, plus an interference term between the 1b and the 2b currents, plus a response due solely to the MEC. Typically, the interference term dominates over the pure MEC contribution, as the MEC represent a small perturbation relative to the one-body current;

$$R^T = R_{1b}^T + R_{1b2b}^T + R_{2b}^T. \quad (20)$$

In this work, we focus on the transverse interference response between 1b and 2b currents R_{1b2b}^T . We will demonstrate the low momentum theorems in the non-relativistic limit. (the contribution of the MEC in the longitudinal channel is of higher order in the non-relativistic limit and can be neglected).

In the non-relativistic limit, the 1b current is the sum of magnetization and convection currents:

$$\mathbf{j}_{1b}(\mathbf{p}, \mathbf{h}) = \mathbf{j}_M(\mathbf{p}, \mathbf{h}) + \mathbf{j}_C(\mathbf{p}, \mathbf{h}), \quad (21)$$

$$\mathbf{j}_M(\mathbf{p}, \mathbf{h}) = -\delta_{t_p t_h} \frac{G_M^h}{2m_N} i\mathbf{q} \times \boldsymbol{\sigma}_{s_p s_h}, \quad (22)$$

$$\mathbf{j}_C(\mathbf{p}, \mathbf{h}) = \delta_{t_p t_h} \delta_{s_p s_h} \frac{G_E^h}{m_N} \left(\mathbf{h} + \frac{\mathbf{q}}{2}\right). \quad (23)$$

with $\mathbf{q} = \mathbf{p} - \mathbf{h}$ by momentum conservation. Here G_M^h (G_E^h) is the magnetic (electric) form factor of the nucleon with isospin t_h . In the quasielastic peak the convection current contribution is much smaller than the magnetization and can be neglected.

B. Meson exchange currents

The starting point in this work is the relativistic MEC model from reference [53], derived from the pion production model of [54], that follows from the Lagrangian given in Appendix A. This model has been used to describe the 2p2h response in both electron and neutrino scattering [17], and has been implemented in the neutrino event generator code GENIE [55]. We begin with the relativistic MEC model and systematically derive its non-relativistic reduction. This approach ensures consistency between relativistic and non-relativistic currents. Additionally, it allows us to connect our results with previous studies that employed non-relativistic calculations, facilitating a direct comparison and validation of our approach. The non-relativistic MEC will serve as the basis for deriving the low-momentum theorems for the 1p1h transverse response in the low momentum transfer regime, allowing us to connect with previous works using non-relativistic models. We consider low momentum transfer to be around $q \sim 500$ MeV/c or lower.

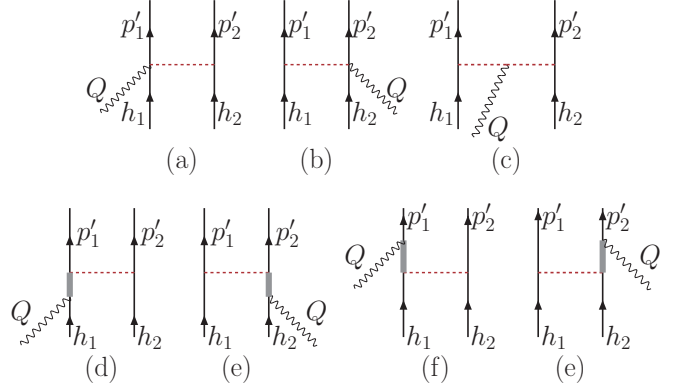


FIG. 1: Feynman diagrams for the MEC model used in this work: seagull (a,b), pion-in-flight (c) and Δ (d,e,f,g).

The relativistic MEC are obtained as the sum of the diagrams depicted in Fig. 1, which include seagull (s), pion-in-flight (π), and Δ isobar currents.

$$j_{2b}^\mu(\mathbf{p}'_1, \mathbf{p}'_2, \mathbf{p}_1, \mathbf{p}_2) = j_s^\mu + j_\pi^\mu + j_\Delta^\mu, \quad (24)$$

where the Δ current is the sum of forward and backward terms

$$j_\Delta^\mu = j_{\Delta F}^\mu + j_{\Delta B}^\mu. \quad (25)$$

The specific treatment of the Δ current is model-dependent, and various versions exist due to uncertainty

in the off-shell properties of the Δ and its interaction with the medium. Other models used for relativistic MEC include those described in Refs. [26, 40, 56], although the 1p1h transverse response does not differ significantly between them and the model presented here. In par-

ticular, a recent calculation [41] of 1p1h responses with the present MEC model was compared with those of the model of Ref. [40], and very similar results were found.

The MEC matrix elements in the present model are given by

$$j_{sea}^\mu = i[\boldsymbol{\tau}^{(1)} \times \boldsymbol{\tau}^{(2)}]_z \frac{f^2}{m_\pi^2} V(1', 1) F_{\pi NN}(k_1^2) \bar{u}_{s_2'}(p_2') F_1^V \gamma^5 \gamma^\mu u_{s_2}(p_2) + (1 \leftrightarrow 2) \quad (26)$$

$$j_\pi^\mu = i[\boldsymbol{\tau}^{(1)} \times \boldsymbol{\tau}^{(2)}]_z \frac{f^2}{m_\pi^2} F_1^V V(1', 1) V(2', 2) (k_1^\mu - k_2^\mu) \quad (27)$$

$$j_{\Delta F}^\mu = U_F(1, 2) \frac{f f^*}{m_\pi^2} V(2', 2) F_{\pi N \Delta}(k_2^2) \bar{u}_{s_1'}(p_1') k_2^\alpha G_{\alpha\beta}(p_1 + Q) \Gamma^{\beta\mu}(Q) u_{s_1}(p_1) + (1 \leftrightarrow 2) \quad (28)$$

$$j_{\Delta B}^\mu = U_B(1, 2) \frac{f f^*}{m_\pi^2} V(2', 2) F_{\pi N \Delta}(k_2^2) \bar{u}_{s_1'}(p_1') k_2^\beta \Gamma^{\alpha\mu}(-Q) G_{\alpha\beta}(p_1' - Q) u_{s_1}(p_1) + (1 \leftrightarrow 2). \quad (29)$$

Here a matrix element between initial and final isospin states is implicit, i.e., $\langle t_1' t_2' | j^\mu | t_1 t_2 \rangle$, although we do not explicitly write this to simplify the notation. The symbols appearing in the MEC matrix elements are the following:

- The πN coupling constant, $f^2 = 1$, and the $\pi N \Delta$ coupling constant, $f^* = 2.13f$.
- The spinors $u(p)$ are the solutions of the Dirac equation with momentum \mathbf{p} .
- The four-vector $k_i^\mu = p_i^\mu - p_i'^\mu$ is the momentum transferred to the nucleon $i = 1, 2$.
- $\boldsymbol{\tau}^{(i)}$ is the isospin operator of nucleon i .
- $F_1^V(Q^2) = F_1^p - F_1^n$ is the isovector form factor of the nucleon.
- The following function of spin and momentum is common to all the currents, including a πNN form factor, and the pion propagator

$$V(1', 1) \equiv F_{\pi NN}(k_1^2) \frac{\bar{u}_{s_1'}(p_1') \gamma^5 \not{k}_1 u_{s_1}(p_1)}{k_1^2 - m_\pi^2}. \quad (30)$$

- The πNN and $\pi N \Delta$ form factors at the pion absorption/emission vertices are [24, 57]

$$F_{\pi NN}(k) = F_{\pi N \Delta}(k) = \frac{\Lambda^2 - m_\pi^2}{\Lambda^2 - k^2}, \quad (31)$$

where the parameter Λ is typically chosen to be around 1300 MeV [58].

The forward Δ current corresponds to processes where the Δ resonance is produced and then decays back to a nucleon, while the backward Δ current involves the

exchange of a pion, leading to the creation of a Δ resonance in the intermediate state. The charge dependence of these processes is embedded in the isospin operators

$$U_F(1, 2) = \sqrt{\frac{3}{2}} \sum_{i=1}^3 T_i^{(1)} T_z^{(1)\dagger} \tau_i^{(2)}, \quad (32)$$

$$U_B(1, 2) = \sqrt{\frac{3}{2}} \sum_{i=1}^3 T_z^{(1)} T_i^{(1)\dagger} \tau_i^{(2)}, \quad (33)$$

where T_i^\dagger are the Cartesian coordinates of the $\frac{1}{2} \rightarrow \frac{3}{2}$ transition isospin operator, defined by [51]

$$\langle \frac{3}{2} t_\Delta | T_\mu^\dagger | \frac{1}{2} t \rangle = \langle \frac{1}{2} t_1 \mu | \frac{3}{2} t_\Delta \rangle \quad (34)$$

T_μ^\dagger being the spherical components of the vector \vec{T}^\dagger .

The following $\gamma N \rightarrow \Delta$ transition vertex [54, 59] is used as the leading contribution for low momentum transfer

$$\Gamma^{\beta\mu}(Q) = \frac{C_3^V}{m_N} (g^{\beta\mu} \not{Q} - Q^\beta \gamma^\mu) \gamma_5. \quad (35)$$

We use the Δ vector form factor [54]:

$$C_3^V(Q^2) = \frac{2.13}{(1 - \frac{Q^2}{M_\Delta^2})^2} \frac{1}{1 - \frac{Q^2}{4M_\Delta^2}}. \quad (36)$$

The Δ propagator is

$$G_{\alpha\beta}(P) = \frac{\mathcal{P}_{\alpha\beta}(P)}{P^2 - M_\Delta^2 + iM_\Delta \Gamma(P^2) + \frac{\Gamma(P^2)^2}{4}} \quad (37)$$

where M_Δ and Γ are the Δ mass and width respectively. The projector $\mathcal{P}_{\alpha\beta}(P)$ over spin-3/2 is

$$\mathcal{P}_{\alpha\beta}(P) = -(P + M_\Delta) \times \left[g_{\alpha\beta} - \frac{\gamma_\alpha \gamma_\beta}{3} - \frac{2P_\alpha P_\beta}{3M_\Delta^2} + \frac{P_\alpha \gamma_\beta - P_\beta \gamma_\alpha}{3M_\Delta} \right] \quad (38)$$

The Δ width $\Gamma(P^2)$ is given by

$$\Gamma(P^2) = \Gamma_0 \frac{m_\Delta}{\sqrt{P^2}} \left(\frac{p_\pi}{p_\pi^{res}} \right)^3. \quad (39)$$

where $\Gamma_0 = 120$ MeV is the Δ width at rest, p_π is the momentum of the final pion in the Δ decay, and p_π^{res} is its value at resonance ($P^2 = m_\Delta^2$).

Some details about the treatment of the Δ propagator, which are model-dependent and not entirely established, are not relevant in the non-relativistic limit considered here but can be significant when applying a relativistic model or making relativistic corrections. The width Γ_Δ corresponds to the Δ in vacuum, and it is expected to be slightly different in the medium depending on the kinematics. Various alternative approximations to the Δ propagator have been proposed. However, in the case of the quasielastic peak, the typical kinematics are of the order of 1 GeV, and these issues are not expected to be relevant. They are overshadowed by other more significant nuclear effects that dominate in this energy regime.

In the non-relativistic limit, which we focus on in this work, these model-dependent details of the Δ propagator are not critical. The primary concern is ensuring that our non-relativistic reduction of the MEC operators is consistent with the standard non-relativistic MEC operators used in previous studies. This consistency guarantees that our results are reliable and can be reproduced using the same theoretical framework.

C. Non relativistic MEC

In this section, we derive in detail the non-relativistic reduction of the meson exchange currents (MEC). This treatment is deliberately didactic, as mentioned, to ensure that our results are easily reproducible. We aim to leave no ambiguous or unclear steps in the derivation process. We will take the static limit in which the momenta of the initial and final nucleons are very small.

In the non-relativistic limit, the lower component of the Dirac spinors is neglected, and the 4×4 Dirac matrices reduce to 2×2 Pauli matrices acting on the upper components. Additionally, we will only consider the non-relativistic reduction of the transverse current, i.e., J^i for $i = 1, 2$, as this is the dominant contribution in this limit. The contribution of MEC to the longitudinal response is neglected as it is of higher order in the non-relativistic limit.

The non-relativistic approximation is further justified by numerical calculations. Although it is not the goal of this article to perform an exhaustive comparison of the longitudinal response R_L in the fully relativistic model, numerical verification shows that the contribution of MEC to R_L is indeed negligible compared to its contribution to the transverse response.

To achieve this reduction, we apply the following rules:

$$\gamma^0 \longrightarrow 1, \quad \gamma^i \longrightarrow 0, \quad \gamma_5 \gamma^0 \longrightarrow 0, \quad (40)$$

$$\gamma_5 \gamma^i \longrightarrow -\sigma_i, \quad \gamma^i \gamma^j \longrightarrow -\sigma_i \sigma_j, \quad \gamma^0 \gamma^j \longrightarrow 0. \quad (41)$$

For a nucleon momentum:

$$p^\mu \longrightarrow (m_N, p^i), \quad \not{p} \longrightarrow p_0 \quad (42)$$

For the momentum transfer to nucleon i :

$$k^\mu \longrightarrow (0, k^i), \quad \gamma_5 \not{k} \longrightarrow \mathbf{k} \cdot \boldsymbol{\sigma}. \quad (43)$$

To simplify the writing at this stage, we do not explicitly include the strong form factors. These can be applied later on to the non-relativistic currents. Most of the results will be obtained with these form factors set to one, and we will see that the effect of including them is small for the low momentum transfer values considered here. Additionally, their inclusion does not alter the sign of the interference.

The V -function of Eq. (30) is directly obtained in this limit

$$V(1', 1) \longrightarrow -\frac{\mathbf{k}_1 \cdot \boldsymbol{\sigma}^{(1)}}{\mathbf{k}_1^2 + m_\pi^2} \quad (44)$$

where a matrix element between initial and final spin states is understood, i.e. $\langle s'_1 | \cdot | s_1 \rangle$, but is not explicitly written for simplicity. The spin states $|s\rangle$ are non-relativistic, two-component spinors, corresponding to the upper component of the Dirac spinors.

1. Seagull current

In the seagull current, we start by using a notation to separate the isospin part, which does not change in the non-relativistic limit, from the spin-momentum part, which does change.

$$j_s^\mu = i[\boldsymbol{\tau}^{(1)} \times \boldsymbol{\tau}^{(2)}]_z (K_s^\mu - L_s^\mu) \quad (45)$$

$$= i[\boldsymbol{\tau}^{(1)} \times \boldsymbol{\tau}^{(2)}]_z j_{s3}^\mu. \quad (46)$$

Here the auxiliary functions K_s^μ , L_s^μ and j_{s3}^μ are independent on isospin and are defined by

$$K_s^\mu(1', 2', 1, 2) = \frac{f^2}{m_\pi^2} V(1', 1) \bar{u}(2') F_1^V \gamma^5 \gamma^\mu u(2) \quad (47)$$

$$L_s^\mu(1', 2', 1, 2) = K_s^\mu(2', 1', 2, 1) \quad (48)$$

$$j_{s3}^\mu = K_s^\mu - L_s^\mu, \quad (49)$$

where in the $(1 \leftrightarrow 2)$ term we have used the property

$$[\boldsymbol{\tau}^{(2)} \times \boldsymbol{\tau}^{(1)}] = -[\boldsymbol{\tau}^{(1)} \times \boldsymbol{\tau}^{(2)}]. \quad (50)$$

The non-relativistic reduction is directly obtained using Eqs. (41) and (44)

$$K_s^i \rightarrow \frac{f^2}{m_\pi^2} F_1^V \frac{\mathbf{k}_1 \cdot \boldsymbol{\sigma}^{(1)}}{\mathbf{k}_1^2 + m_\pi^2} \sigma_i^{(2)} \quad (51)$$

where, as before, a matrix element between two-components initial and final spin states is understood, $\langle s'_1 s'_2 | \cdot | s_1 s_2 \rangle$. Therefore the spin-momentum part of the seagull current j_{s3}^i in the NR limit becomes

$$\mathbf{j}_{s3} \rightarrow \frac{f^2}{m_\pi^2} F_1^V \left(\frac{\mathbf{k}_1 \cdot \boldsymbol{\sigma}^{(1)}}{\mathbf{k}_1^2 + m_\pi^2} \boldsymbol{\sigma}^{(2)} - \frac{\mathbf{k}_2 \cdot \boldsymbol{\sigma}^{(2)}}{\mathbf{k}_2^2 + m_\pi^2} \boldsymbol{\sigma}^{(1)} \right). \quad (52)$$

2. Pionic current

The pion-in-flight current can be written similarly to the seagull current as

$$j_\pi^\mu = i[\boldsymbol{\tau}^{(1)} \times \boldsymbol{\tau}^{(2)}]_z j_{\pi 3}^\mu \quad (53)$$

where $j_{\pi 3}^\mu$ is independent on isospin and is defined by

$$j_{\pi 3}^\mu(1', 2', 1, 2) = \frac{f^2}{m_\pi^2} F_1^V V(1', 1) V(2', 2) (k_1^\mu - k_2^\mu). \quad (54)$$

The non-relativistic reduction of the seagull current is directly obtained from Eq. (44)

$$\mathbf{j}_{\pi 3} \rightarrow \frac{f^2}{m_\pi^2} F_1^V \frac{\mathbf{k}_1 \cdot \boldsymbol{\sigma}^{(1)}}{\mathbf{k}_1^2 + m_\pi^2} \frac{\mathbf{k}_2 \cdot \boldsymbol{\sigma}^{(2)}}{\mathbf{k}_2^2 + m_\pi^2} (\mathbf{k}_1 - \mathbf{k}_2). \quad (55)$$

It is straightforward to verify that the non-relativistic reduction of the seagull plus pionic currents coincide with the usual expressions found in the literature [48].

3. Δ current

The NR reduction of the Δ current is somewhat more involved due to its more complex spin and isospin structure. This complexity arises from the transition between nucleon and Δ states, and the Δ propagator, which introduces additional terms that must be carefully managed during the non-relativistic limit process. In order to simplify the non-relativistic reduction, it is convenient to write the Δ current in an abbreviated form

$$j_{\Delta F}^\mu = U_F K_F^\mu + (1 \leftrightarrow 2) \quad (56)$$

$$j_{\Delta B}^\mu = U_B K_B^\mu + (1 \leftrightarrow 2) \quad (57)$$

where a matrix element is assumed to be taken between the initial and final isospin states $\langle t'_1 t'_2 | \cdot | t_1 t_2 \rangle$, but we do not explicitly write this to simplify the notation.

The functions K_F^μ and K_B^μ are independent on isospin and can be written as

$$K_F^\mu = \frac{f f^*}{m_\pi^2} V(2', 2) A^\mu, \quad (58)$$

$$K_B^\mu = \frac{f f^*}{m_\pi^2} V(2', 2) B^\mu. \quad (59)$$

Finally A^μ and B^μ are defined as

$$A^\mu = \bar{u}(1') k_2^\alpha G_{\alpha\beta}(p_1 + Q) \Gamma^{\beta\mu}(Q) u(1) \quad (60)$$

$$B^\mu = \bar{u}(1') k_2^\beta \Gamma^{\alpha\mu}(-Q) G_{\alpha\beta}(p'_1 - Q) u(1). \quad (61)$$

The non-relativistic reduction of the spatial components of the Δ current requires the non-relativistic reduction of the components A^i and B^i . This detailed reduction process is carried out in Appendix B. The result is

$$\mathbf{A} \rightarrow g_\Delta \mathbf{q} \times \left[\frac{2}{3} i \mathbf{k}_2 - \frac{1}{3} \mathbf{k}_2 \times \boldsymbol{\sigma}^{(1)} \right] \quad (62)$$

$$\mathbf{B} \rightarrow g_\Delta \mathbf{q} \times \left[\frac{2}{3} i \mathbf{k}_2 + \frac{1}{3} \mathbf{k}_2 \times \boldsymbol{\sigma}^{(1)} \right], \quad (63)$$

where we have defined the constant

$$g_\Delta \equiv \frac{c_3^V}{m_N} \frac{1}{m_\Delta - m_N}. \quad (64)$$

Therefore

$$\mathbf{K}_F \rightarrow -\frac{f f^*}{m_\pi^2} \frac{\mathbf{k}_2 \cdot \boldsymbol{\sigma}^{(2)}}{\mathbf{k}_2^2 + m_\pi^2} \mathbf{A} \quad (65)$$

$$\mathbf{K}_B \rightarrow -\frac{f f^*}{m_\pi^2} \frac{\mathbf{k}_2 \cdot \boldsymbol{\sigma}^{(2)}}{\mathbf{k}_2^2 + m_\pi^2} \mathbf{B}. \quad (66)$$

As before, a matrix element is assumed to be taken between the initial and final spin states, $\langle s'_1 s'_2 | \cdot | s_1 s_2 \rangle$, but we do not explicitly write this to simplify the notation.

Using the result

$$T_i T_j^\dagger = \frac{2}{3} \delta_{ij} - \frac{i}{3} \epsilon_{ijk} \tau_k = \delta_{ij} - \frac{1}{3} \tau_i \tau_j \quad (67)$$

the forward and backward isospin operators can be written as

$$U_F(1, 2) = \frac{1}{\sqrt{6}} \left(2\tau_z^{(2)} - i[\boldsymbol{\tau}^{(1)} \times \boldsymbol{\tau}^{(2)}]_z \right) \quad (68)$$

$$U_B(1, 2) = \frac{1}{\sqrt{6}} \left(2\tau_z^{(2)} + i[\boldsymbol{\tau}^{(1)} \times \boldsymbol{\tau}^{(2)}]_z \right). \quad (69)$$

Hence the Δ current can be written as

$$\begin{aligned} \mathbf{j}_\Delta &= \mathbf{j}_{\Delta F} + \mathbf{j}_{\Delta B} \\ &= \frac{2}{\sqrt{6}} \tau_z^{(2)} [\mathbf{K}_F + \mathbf{K}_B] \\ &\quad + \frac{1}{\sqrt{6}} i[\boldsymbol{\tau}^{(1)} \times \boldsymbol{\tau}^{(2)}]_z [\mathbf{K}_B - \mathbf{K}_F] + (1 \leftrightarrow 2). \end{aligned} \quad (70)$$

We see that the isospin operators in the Δ current, $\tau_z^{(2)}$ and $[\boldsymbol{\tau}^{(1)} \times \boldsymbol{\tau}^{(2)}]_z$, are multiplied by the sum and the difference between the backward and forward functions, \mathbf{K}_B and \mathbf{K}_F , given in the NR limit by

$$\mathbf{K}_F + \mathbf{K}_B = -\frac{f f^*}{m_\pi^2} \frac{\mathbf{k}_2 \cdot \boldsymbol{\sigma}^{(2)}}{\mathbf{k}_2^2 + m_\pi^2} (\mathbf{A} + \mathbf{B}) \quad (71)$$

$$\mathbf{K}_B - \mathbf{K}_F = -\frac{f f^*}{m_\pi^2} \frac{\mathbf{k}_2 \cdot \boldsymbol{\sigma}^{(2)}}{\mathbf{k}_2^2 + m_\pi^2} (\mathbf{B} - \mathbf{A}). \quad (72)$$

From Eqs. (62) and (63),

$$\mathbf{A} + \mathbf{B} = \frac{4}{3} g_\Delta i \mathbf{q} \times \mathbf{k}_2 \quad (73)$$

$$\mathbf{B} - \mathbf{A} = \frac{2}{3} g_\Delta \mathbf{q} \times (\mathbf{k}_2 \times \boldsymbol{\sigma}^{(1)}). \quad (74)$$

Inserting this result into Eqs. (71) and (72) we have

$$\mathbf{K}_F + \mathbf{K}_B = -\frac{4}{3}g_\Delta \frac{ff^*}{m_\pi^2} \frac{\mathbf{k}_2 \cdot \boldsymbol{\sigma}^{(2)}}{\mathbf{k}_2^2 + m_\pi^2} i\mathbf{q} \times \mathbf{k}_2, \quad (75)$$

$$\mathbf{K}_B - \mathbf{K}_F = -\frac{2}{3}g_\Delta \frac{ff^*}{m_\pi^2} \frac{\mathbf{k}_2 \cdot \boldsymbol{\sigma}^{(2)}}{\mathbf{k}_2^2 + m_\pi^2} \mathbf{q} \times (\mathbf{k}_2 \times \boldsymbol{\sigma}^{(1)}). \quad (76)$$

$$\mathbf{j}_\Delta = i\sqrt{\frac{3}{2}} \frac{2ff^*}{9} \frac{c_3^V}{m_\pi^2} \frac{1}{m_N m_\Delta - m_N} \left\{ \frac{\mathbf{k}_2 \cdot \boldsymbol{\sigma}^{(2)}}{\mathbf{k}_2^2 + m_\pi^2} \left[4\tau_z^{(2)}\mathbf{k}_2 + [\boldsymbol{\tau}^{(1)} \times \boldsymbol{\tau}^{(2)}]_z \mathbf{k}_2 \times \boldsymbol{\sigma}^{(1)} \right] \right. \\ \left. + \frac{\mathbf{k}_1 \cdot \boldsymbol{\sigma}^{(1)}}{\mathbf{k}_1^2 + m_\pi^2} \left[4\tau_z^{(1)}\mathbf{k}_1 - [\boldsymbol{\tau}^{(1)} \times \boldsymbol{\tau}^{(2)}]_z \mathbf{k}_1 \times \boldsymbol{\sigma}^{(2)} \right] \right\} \times \mathbf{q}. \quad (77)$$

One can, in fact, verify that this expression coincides with the Δ current appearing in the literature, particularly the expression given in Refs. [48, 49], that we use as reference, except for the precise values of the coupling constants and form factors. This assures us that the relativistic and non-relativistic calculations in the low-momentum and low-energy limit should coincide if identical values of coupling and form factors are used.

D. MEC effective one-body transition currents

With the non-relativistic MEC current obtained in the last section, In the non-relativistic limit, the effective one-body transition current $\mathbf{j}_{2b}(\mathbf{p}, \mathbf{h})$ in the Fermi gas is obtained by summing over the spin, isospin, and integrating over the momentum k of the spectator nucleon. At leading order, only the spatial part of the MEC survives, affecting solely the transverse response, which is perpendicular to the transferred momentum \mathbf{q} . From Eq. (10) in the $V \rightarrow \infty$ this current is

$$\mathbf{j}_{2b}(\mathbf{p}, \mathbf{h}) = \int \frac{d^3k}{(2\pi)^3} \sum_{t_k s_k} [\mathbf{j}_{2b}(p, k, h, k) - \mathbf{j}_{2b}(p, k, k, h)]. \quad (78)$$

1. Sum over isospin

We begin by showing that the direct term in Eq. (78) is zero. Previously, we note that the MEC can be expanded in terms of the isospin operators $\tau_z^{(1)}$, $\tau_z^{(2)}$ and $[\boldsymbol{\tau}^{(1)} \times \boldsymbol{\tau}^{(2)}]_z$

$$\mathbf{j}_{2b} = \tau_z^{(1)}\mathbf{j}_1 + \tau_z^{(2)}\mathbf{j}_2 + i[\boldsymbol{\tau}^{(1)} \times \boldsymbol{\tau}^{(2)}]_z \mathbf{j}_3 \quad (79)$$

where \mathbf{j}_1 , \mathbf{j}_2 , \mathbf{j}_3 are independent on isospin.

Using these results in Eq. (70), it is straightforward to obtain the following expression for the NR Δ current

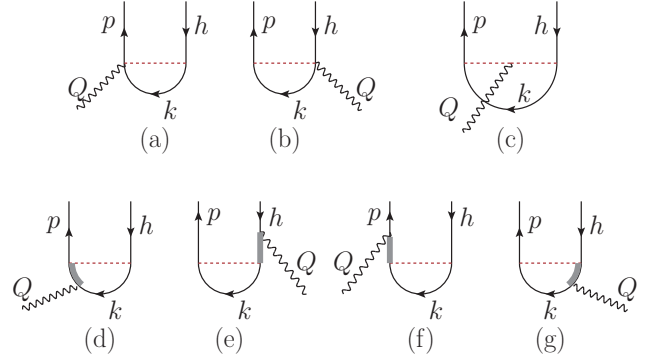


FIG. 2: Many-body diagrams for the 1p1h MEC matrix elements

We first perform the sum over isospin index t_k . The direct term is

$$\sum_{t_k} \mathbf{j}_{2b}(p, k, h, k) = \sum_{t_k} \langle t_p t_k | \tau_z^{(1)}\mathbf{j}_1 + \tau_z^{(2)}\mathbf{j}_2 + \\ + i[\boldsymbol{\tau}^{(1)} \times \boldsymbol{\tau}^{(2)}]_z \mathbf{j}_3 | t_h t_k \rangle \\ = \delta_{t_p t_h} 4t_h \mathbf{j}_1(p, k, h, k), \quad (80)$$

where we have used the elementary isospin sums performed in Appendix C, Eqs. (C5–C7) Therefore the direct term in the matrix element (78) is proportional to $\mathbf{j}_1(\mathbf{p}, \mathbf{k}, \mathbf{h}, \mathbf{k})$, which turns out to be zero. Indeed, \mathbf{j}_1 can be obtained from equation (77) as

$$\mathbf{j}_1 = iC_\Delta \frac{\mathbf{k}_1 \cdot \boldsymbol{\sigma}^{(1)}}{\mathbf{k}_1^2 + m_\pi^2} 4\mathbf{k}_1 \times \mathbf{q}, \quad (81)$$

with

$$C_\Delta \equiv \sqrt{\frac{3}{2}} \frac{2ff^*}{9} \frac{C_3^V}{m_\pi^2} \frac{1}{m_N m_\Delta - m_N} \quad (82)$$

and $\mathbf{k}_1 = \mathbf{p} - \mathbf{h} = \mathbf{q}$. Therefore

$$\sum_{t_k} \mathbf{j}_{2b}(p, k, h, k) = 0. \quad (83)$$

This results follows because the Δ current is transverse,

i.e., perpendicular to \mathbf{q} . In the relativistic case, a similar situation occurs, and the direct term is zero although the demonstration is more involved. It requires summing over the spin of \mathbf{k} and handling a large number of terms that involve many γ matrices.

The sum over isospin in the exchange part is obtained using the isospin sums performed in Appendix C, Eqs (C8–C10)

$$\begin{aligned} \sum_{t_k} \mathbf{j}_{2b}(p, k, k, h) &= \sum_{t_k = \pm 1/2} \langle t_p t_k | \tau_z^{(1)} \mathbf{j}_1 + \tau_z^{(2)} \mathbf{j}_2 + i[\boldsymbol{\tau}^{(1)} \times \boldsymbol{\tau}^{(2)}]_z \mathbf{j}_3 | t_k t_h \rangle \\ &= \delta_{t_p t_h} 2t_h [\mathbf{j}_1(p, k, k, h) + \mathbf{j}_2(p, k, k, h) - 2\mathbf{j}_3(p, k, k, h)]. \end{aligned} \quad (84)$$

Here we observe that in symmetric nuclear matter, the direct matrix element of the MEC vanishes, and only the exchange term survives in the 1p1h matrix element. Therefore, the many-body diagrams that contribute to the MEC in the 1p1h channel are those shown in Fig. 2. Next, we proceed to perform the spin sums for the different terms of the current.

It can be shown that, in fact, two of the four exchange diagrams contributing to the Δ current in the 1p1h matrix element are zero. Specifically, due to the sum over isospin in the forward Δ current, the diagram containing the isospin operator $U_F(2, 1)$ yields zero (diagram (e) of Fig. 2). Similarly, for the backward Δ current, the diagram involving the isospin operator $U_B(1, 2)$ also vanishes (diagram (f) of Fig. 2). Therefore only diagrams (d), forward, and (g), backward, contribute in the case of the Δ current. These results are demonstrated in Appendix B.

2. Sum over spin

The resulting 1p1h matrix elements of the 2b current are computed as

$$\mathbf{j}_{2b}(p, h) = - \int \frac{d^3 k}{(2\pi)^3} \sum_{t_k s_k} \mathbf{j}_{2b}(p, k, k, h) = \mathbf{j}_s(p, h) + \mathbf{j}_\pi(p, h) + \mathbf{j}_\Delta(p, h), \quad (85)$$

where only the exchange part contributes. The sums over spin index s_k are performed in Appendix D. The results are the following for the three MEC, seagull, pionic and Δ currents

$$\mathbf{j}_s(p, h) = 4t_h \delta_{t_p t_h} \frac{f^2}{m_\pi^2} F_1^V \int \frac{d^3 k}{(2\pi)^3} \left(\frac{\delta_{s_p s_h} \mathbf{k}_1 + i \boldsymbol{\sigma}_{ph} \times \mathbf{k}_1}{\mathbf{k}_1^2 + m_\pi^2} - \frac{\delta_{s_p s_h} \mathbf{k}_2 + i \mathbf{k}_2 \times \boldsymbol{\sigma}_{ph}}{\mathbf{k}_2^2 + m_\pi^2} \right) \quad (86)$$

$$\mathbf{j}_\pi(p, h) = 4t_h \delta_{t_p t_h} \frac{f^2}{m_\pi^2} F_1^V \int \frac{d^3 k}{(2\pi)^3} \frac{\delta_{s_p s_h} \mathbf{k}_1 \cdot \mathbf{k}_2 + i(\mathbf{k}_1 \times \mathbf{k}_2) \cdot \boldsymbol{\sigma}_{ph}}{(\mathbf{k}_1^2 + m_\pi^2)(\mathbf{k}_2^2 + m_\pi^2)} (\mathbf{k}_1 - \mathbf{k}_2) \quad (87)$$

$$\mathbf{j}_\Delta(p, h) = 4it_h \delta_{t_p t_h} C_\Delta \mathbf{q} \times \int \frac{d^3 k}{(2\pi)^3} \left(\frac{\mathbf{k}_1^2 \boldsymbol{\sigma}_{ph} + (\boldsymbol{\sigma}_{ph} \cdot \mathbf{k}_1) \mathbf{k}_1}{\mathbf{k}_1^2 + m_\pi^2} + \frac{\mathbf{k}_2^2 \boldsymbol{\sigma}_{ph} + (\boldsymbol{\sigma}_{ph} \cdot \mathbf{k}_2) \mathbf{k}_2}{\mathbf{k}_2^2 + m_\pi^2} \right) \quad (88)$$

with $\mathbf{k}_1 = \mathbf{p} - \mathbf{k}$ and $\mathbf{k}_2 = \mathbf{k} - \mathbf{h}$.

E. Interference between one-body and MEC in the transverse response

In this section, we give the MEC contribution to the effective single-nucleon transverse response, focusing exclusively on the interference between the MEC and OB currents. The pure MEC responses have been previously computed and shown in various studies to be negligible, allowing them to be safely disregarded. Here, we describe the interference terms separately for the different MEC

components: Seagull, pionic, and Δ , in combination with the magnetization and convection terms of the OB currents. This separation is essential to analyze the relative contributions of each component to the overall response.

It should be clarified that here we are computing the single-nucleon response corresponding to either a proton or a neutron, with the requirement that the isospin of p and h must be the same $t_p = t_h$. At the end of the calculation, the contributions from protons and neutrons must be summed to obtain the total response.

The magnetization-seagull (ms) interference is given by Eq. (18)

$$w_{ms}^T = w_{ms}^{11} + w_{ms}^{22} = \text{Re} \sum \mathbf{j}_m(p, h)^* \cdot \mathbf{j}_s(p, h) \quad (89)$$

where we use that the magnetization current is perpendicular to \mathbf{q} and it has only x, y components. Using Eq. (22) for the magnetization current we can write

$$\begin{aligned} w_{ms}^T &= \delta_{t_p t_h} \text{Re} \sum_{s_p s_h} \left(-\frac{G_M^h}{2m_N} i \mathbf{q} \times \boldsymbol{\sigma}_{s_p s_h} \right)^* \cdot \mathbf{j}_s(p, h) \\ &= \sum_{s_p s_h} \frac{G_M^h}{2m_N} i (\mathbf{q} \times \boldsymbol{\sigma}_{s_h s_p}) \cdot \mathbf{j}_s(\mathbf{p}, \mathbf{h})_{s_p s_h}. \end{aligned} \quad (90)$$

We have utilized the fact that the spin sum already yields a real number, as will be shown later, making it unnecessary to explicitly take the real part.

By following the same procedure, we express the various interferences required between the convection and magnetization currents with the seagull, pionic, and Δ operators, as follows:

$$w_{cs}^T = \text{Re} \sum \mathbf{j}_c^T(p, h)^* \cdot \mathbf{j}_s(p, h) = \sum_{s_p s_h} \frac{G_E^h}{m_N} \delta_{s_h s_p} \mathbf{h}_T \cdot \mathbf{j}_s(\mathbf{p}, \mathbf{h})_{s_p s_h} \quad (91)$$

$$w_{m\pi}^T = \text{Re} \sum \mathbf{j}_m(p, h)^* \cdot \mathbf{j}_\pi(p, h) = \sum_{s_p s_h} \frac{G_M^h}{2m_N} i (\mathbf{q} \times \boldsymbol{\sigma}_{s_h s_p}) \cdot \mathbf{j}_\pi(\mathbf{p}, \mathbf{h})_{s_p s_h}, \quad (92)$$

$$w_{c\pi}^T = \text{Re} \sum \mathbf{j}_c^T(p, h)^* \cdot \mathbf{j}_\pi(p, h) = \sum_{s_p s_h} \frac{G_E^h}{m_N} \delta_{s_h s_p} \mathbf{h}_T \cdot \mathbf{j}_\pi(\mathbf{p}, \mathbf{h})_{s_p s_h} \quad (93)$$

$$w_{m\Delta}^T = \text{Re} \sum \mathbf{j}_m(p, h)^* \cdot \mathbf{j}_\Delta(p, h) = \sum_{s_p s_h} \frac{G_M^h}{2m_N} i (\mathbf{q} \times \boldsymbol{\sigma}_{s_h s_p}) \cdot \mathbf{j}_\Delta(\mathbf{p}, \mathbf{h})_{s_p s_h} \quad (94)$$

$$w_{c\Delta}^T = 0. \quad (95)$$

Note that only the transverse component of the convection current appears that is proportional to the transverse nucleon momentum, $\mathbf{h}_T = \mathbf{h} - \frac{\mathbf{h} \cdot \mathbf{q}}{q^2} \mathbf{q}$, thereby selecting the x and y components in the transverse response. We also anticipate that the convection- Δ interference is zero because the convection current is spin-independent, while the Δ current is linear in the σ operators.

The sums over spin in Eqs. (90–94) are performed in Appendix E.

$$w_{ms}^T(p, h) = 4t_h \frac{f^2}{m_\pi^2} F_1^V \frac{G_M^h}{2m_N} \int \frac{d^3 k}{(2\pi)^3} \left(\frac{4\mathbf{q} \cdot \mathbf{k}_1}{\mathbf{k}_1^2 + m_\pi^2} + \frac{4\mathbf{q} \cdot \mathbf{k}_2}{\mathbf{k}_2^2 + m_\pi^2} \right) \equiv 4t_h \frac{f^2}{m_\pi^2} F_1^V \frac{G_M^h}{2m_N} \mathcal{I}_{ms}(\mathbf{p}, \mathbf{h}) \quad (96)$$

$$w_{cs}^T(p, h) = 4t_h \frac{f^2}{m_\pi^2} F_1^V \frac{G_E^h}{m_N} \int \frac{d^3 k}{(2\pi)^3} \left(\frac{2\mathbf{h}_T \cdot \mathbf{k}_1}{\mathbf{k}_1^2 + m_\pi^2} - \frac{2\mathbf{h}_T \cdot \mathbf{k}_2}{\mathbf{k}_2^2 + m_\pi^2} \right) \equiv 4t_h \frac{f^2}{m_\pi^2} F_1^V \frac{G_E^h}{m_N} \mathcal{I}_{cs}(\mathbf{p}, \mathbf{h}) \quad (97)$$

$$w_{m\pi}^T(p, h) = -4t_h \frac{f^2}{m_\pi^2} F_1^V \frac{G_M^h}{2m_N} \int \frac{d^3 k}{(2\pi)^3} \frac{4(\mathbf{q} \times \mathbf{k}_2)^2}{(\mathbf{k}_1^2 + m_\pi^2)(\mathbf{k}_2^2 + m_\pi^2)} \equiv -4t_h \frac{f^2}{m_\pi^2} F_1^V \frac{G_M^h}{2m_N} \mathcal{I}_{m\pi}(\mathbf{p}, \mathbf{h}) \quad (98)$$

$$w_{c\pi}^T(p, h) = -4t_h \frac{f^2}{m_\pi^2} F_1^V \frac{G_E^h}{m_N} \int \frac{d^3 k}{(2\pi)^3} \frac{4(\mathbf{q} \cdot \mathbf{k}_2 - \mathbf{k}_2^2) \mathbf{h}_T \cdot \mathbf{k}_2}{(\mathbf{k}_1^2 + m_\pi^2)(\mathbf{k}_2^2 + m_\pi^2)} \equiv -4t_h \frac{f^2}{m_\pi^2} F_1^V \frac{G_E^h}{m_N} \mathcal{I}_{c\pi}(\mathbf{p}, \mathbf{h}) \quad (99)$$

$$w_{m\Delta}^T(p, h) = -4t_h C_\Delta \frac{G_M^h}{2m_N} \int \frac{d^3 k}{(2\pi)^3} \frac{3q^2 k_1^2 - (\mathbf{q} \cdot \mathbf{k}_1)^2}{\mathbf{k}_1^2 + m_\pi^2} + \frac{3q^2 k_2^2 - (\mathbf{q} \cdot \mathbf{k}_2)^2}{\mathbf{k}_2^2 + m_\pi^2} \equiv -4t_h C_\Delta \frac{G_M^h}{2m_N} \mathcal{I}_{m\Delta}(\mathbf{p}, \mathbf{h}), \quad (100)$$

where C_Δ is defined in Eq. (82), $\mathbf{k}_1 = \mathbf{p} - \mathbf{k}$ and $\mathbf{k}_2 = \mathbf{k} - \mathbf{h}$. In Eqs. (96–100) we have defined the integrals $\mathcal{I}_{ab}(\mathbf{p}, \mathbf{h})$, that are spin independent.

Finally, the total interference between the one-body and two-body currents is given by the sum of the individual interferences between the different terms of the currents, namely the seagull, pionic, and Delta contributions with magnetization and convection currents.

$$w_{1b2b}^T = w_{ms}^T + w_{cs}^T + w_{m\pi}^T + w_{c\pi}^T + w_{m\Delta}^T. \quad (101)$$

F. Low-momentum theorems

negative in the Fermi gas model: $w_{m\Delta}^T < 0$.

Theorem 1 *The transverse interference response between the Δ current and the one-body (OB) current is*

This theorem is specifically applicable at moderate momentum and energy transfers. "Moderate" in this context refers to values small compared to the nucleon mass.

To demonstrate the theorem, we first need to express the total single-nucleon interference responses as the sum of the contributions from protons and neutrons.

$$w_{ms}^T(\mathbf{p}, \mathbf{h}) = \frac{f^2}{m_\pi^2} F_1^V \frac{G_M^p - G_M^n}{m_N} \mathcal{I}_{ms}(\mathbf{p}, \mathbf{h}) \quad (102)$$

$$w_{cs}^T(\mathbf{p}, \mathbf{h}) = 2 \frac{f^2}{m_\pi^2} F_1^V \frac{G_E^p - G_E^n}{m_N} \mathcal{I}_{cs}(\mathbf{p}, \mathbf{h}) \quad (103)$$

$$w_{m\pi}^T(\mathbf{p}, \mathbf{h}) = -\frac{f^2}{m_\pi^2} F_1^V \frac{G_M^p - G_M^n}{m_N} \mathcal{I}_{m\pi}(\mathbf{p}, \mathbf{h}) \quad (104)$$

$$w_{c\pi}^T(\mathbf{p}, \mathbf{h}) = -2 \frac{f^2}{m_\pi^2} F_1^V \frac{G_E^p - G_E^n}{m_N} \mathcal{I}_{c\pi}(\mathbf{p}, \mathbf{h}) \quad (105)$$

$$w_{m\Delta}^T(\mathbf{p}, \mathbf{h}) = -\sqrt{\frac{3}{2}} \frac{f f^*}{2} \frac{C_3^V}{m_\pi^2 m_N^2} \frac{G_M^p - G_M^n}{m_\Delta - m_N} \mathcal{I}_{m\Delta}(\mathbf{p}, \mathbf{h}). \quad (106)$$

It suffices to verify that the single-nucleon interference response $w_{m\Delta}^T < 0$ in Eq (106). On the one hand, $w_{m\Delta}^T$ is proportional to the integral $\mathcal{I}_{m\Delta}$, which contains the pion propagator multiplied by a factor that is always positive. The term in question can be seen inside the integral of Eq. (100), given by

$$3q^2 k_i^2 - (\mathbf{q} \cdot \mathbf{k}_i)^2 \geq 0, \quad (107)$$

with $i = 1, 2$. This ensures that the integral $\mathcal{I}_{m\Delta} \geq 0$. On the other hand, $w_{m\Delta}^T$ is also proportional to $G_M^p - G_M^n$, which is positive as well. Therefore, since $w_{m\Delta}^T$ includes an overall negative sign, the final result is negative, completing the proof.

Typically, the theorem is valid for momentum transfers below approximately 500 MeV, where the interference response $m\Delta$ is explicitly negative. For momentum transfers above this threshold, relativistic effects become increasingly significant. In this regime, the explicit determination of the sign is no longer straightforward due to the complexity of the spin sum in the relativistic case. The analysis requires numerical computations to verify the sign of the interference, as the non-relativistic theorem no longer applies directly.

From Eq. (98), we can also establish the following theorem for the magnetization-pionic response:

Theorem 2 *The transverse interference response between the pionic current and the magnetization current is negative in the non-relativistic Fermi gas: $w_{m\pi}^T < 0$*

The proof of this theorem follows similarly to Theorem 1, by noticing that the integral $\mathcal{I}_{m\pi}$ is positive, as it contains the square of $\mathbf{q} \times \mathbf{k}_2$, as seen in Eq. (98). Then, according to Eq. (104), we conclude that $w_{m\pi}^T < 0$.

The convection-pionic interference does not generally have a well-defined sign, but its contribution is much smaller than the magnetization interference. Therefore,

Theorem 2 can be approximately extended to the total pionic-OB interference.

For the seagull-magnetization interference, a rigorous result is also difficult to establish. However, certain particular cases suggest a trend. For instance, in the case $\mathbf{h} = 0$, it can be demonstrated that $w_{ms}^T > 0$. Additionally, by analyzing the integrand of \mathcal{I}_{ms} for $\mathbf{k} = 0$, we observe that it remains positive below the quasielastic peak and changes sign for $\omega > (q^2/2m_N)(1 + (2m_\pi/q)^2)^{1/2}$. This suggests a general tendency: the interference starts positive at small ω and eventually changes sign at some point beyond the quasielastic peak, though the precise location cannot be determined analytically.

The integrands and signs in the equations for the ms , $m\pi$, and $m\Delta$ transverse responses are consistent with those in the pioneering work of Kohno and Ohtsuka [36], which was among the first to compute 1b2b interferences using Riska's currents. Similar expressions were also obtained in [38, 39], although written in a different form. One of the key contributions and novelties of the present work is the observation that the signs of the $m\Delta$ and $m\pi$ contributions are evidently negative, which follows trivially from Eqs. (98) and (100), as established in our theorems.

III. RESULTS

Here we present results for the transverse response functions due to the interference between the MEC and OB current in the 1p1h channel. As discussed in the previous sections, these interferences are expressed as an integral of an effective single-nucleon interference. In the non-relativistic Fermi gas, which we have examined in great detail, the single-nucleon interferences are represented through relatively complex integrals after analytically computing the spin traces. In the case of the seagull and Δ currents, these integrals are analytical. For the Δ current, it has been proven that the associated response is always negative for all values of q and ω (Theorem 1). In this results section, we calculate the interference transverse responses for various values of $q = 300, 400, 550$ MeV/c, and show the results as a function of ω for ^{12}C . We employ several nuclear models to compare the responses, primarily aiming to observe if the results deviate or not from the Fermi gas significantly. The nuclear models we use include: non-relativistic Fermi gas, relativistic Fermi gas, mean-field models, semi-relativistic models (both Fermi gas and mean field), and the spectral function model. Relativistic mean field and superscaling models with effective nucleon mass are also considered. The mean-field models include the Woods-Saxon potential, Dirac-equation-based potential, and the plane wave approximation. Many of these models have been previously applied in calculations for the study of electron scattering. Our results show approximate agreement in both magnitude and sign of the different MEC contributions. In particular, all examined

models verify the theorem that the effect of the delta current is negative for these values of momentum transfer, and the total MEC effect is small and predominantly negative. This supports the consensus that models without pn tensor correlations do not produce an enhancement of the transverse response.

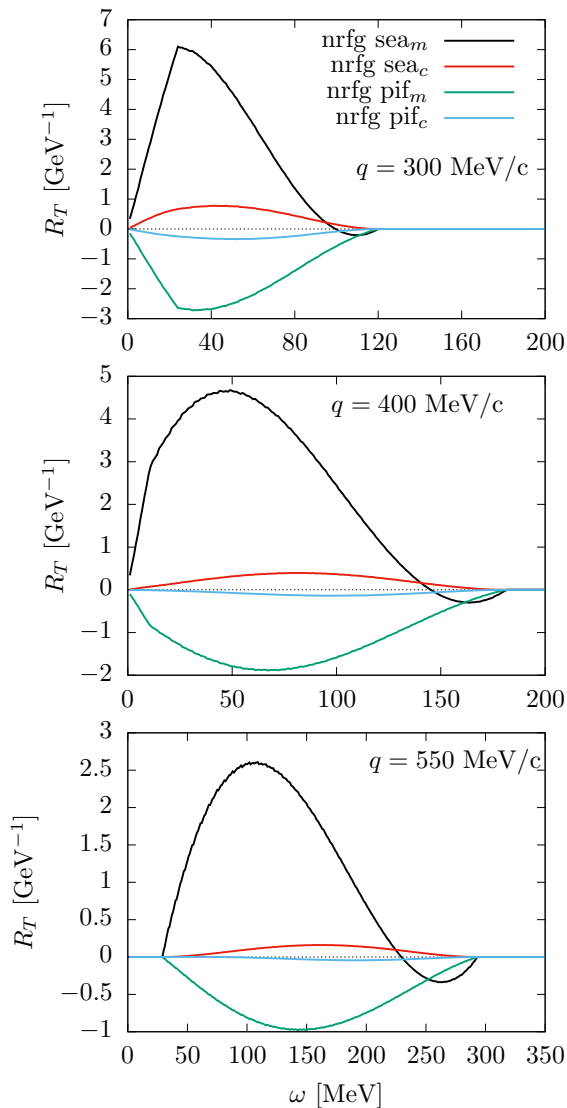


FIG. 3: Interferences between the components of the one-body current and the MEC in the 1p1h transverse response. Specifically, we represent the magnetization-seagull (sea_m), convection-seagull (sea_c), magnetization-pionic (pif_m), and convection-pionic (pif_c) interferences for different values of q .

A. Fermi gas

We begin by presenting in Fig. 3 results for the non-relativistic Fermi gas, with $k_F = 225$ MeV/c. We show the interference of the seagull and pionic currents with the magnetization and convection currents. This is done

to demonstrate that the contribution of the convection current in the MEC-OB interference is very small, particularly in the case of the pionic current. As a result, the magnetization current is dominant in the interference for these low to intermediate momentum transfer values. Specifically, we can conclude that, according to Theorem 2, the contribution of the pionic current is negative if the small convection contribution is disregarded.

Taking this into account, it is worth mentioning the calculation performed by Alberico et al. [37]. In that reference, a positive result was obtained for the pionic-OB interference, which clearly points to an error in the calculation, as it also considered a Fermi gas model. As we have previously discussed, the theorem establishes that this interference is negative when convection is neglected. In fact, by inspecting Eq. (2.41) of Ref. [37], it can be observed that the contribution of the pionic current is positive in that reference, indicating a possible error in performing the spin summation.

In Fig. 4, we present the interferences of the separate MEC components —seagull, pionic, and Δ — with the OB current in the transverse response. Here, we compare the non-relativistic Fermi gas to the relativistic Fermi gas. Both models yield similar results, with increasing differences as the momentum transfer increases, primarily due to the different kinematics. In fact, it can be checked that the relativistic result converges numerically to the non-relativistic one when both the momentum transfer q and the Fermi momentum approach zero [41]. Non-relativistic responses extend to higher values of ω , due to the kinematics. We observe that both Theorems 1 and 2 remain valid in the relativistic case, even though they were proven in the non-relativistic limit.

B. Mean field with Woods-Saxon potential

In Fig. 5, we compare the Fermi gas results to those of the mean field model for finite nuclei, using a Woods-Saxon (WS) potential [38, 39]. In this model, the initial and final nucleon states are solutions to the Schrödinger equation

$$\left[-\frac{1}{2m_N} \nabla^2 + V(r) \right] \psi(\mathbf{r}) = \epsilon \psi(\mathbf{r}), \quad (108)$$

for positive and negative values of the energy ϵ . The WS potential is given by

$$V(r) = -V_0 f(r) + \left(\frac{\hbar}{m_\pi c} \right)^2 \frac{\mathbf{l} \cdot \boldsymbol{\sigma}}{r} \frac{df}{dr} + V_C(r), \quad (109)$$

where the function $f(r)$ is the standard Woods-Saxon shape function

$$f(r) = \frac{1}{1 + e^{(r-R)/a}}, \quad (110)$$

and $V_C(r)$ is the Coulomb potential of a homogeneously charged sphere with radius R . For ^{12}C we use the WS parameters for ^{12}C given in Table 1.

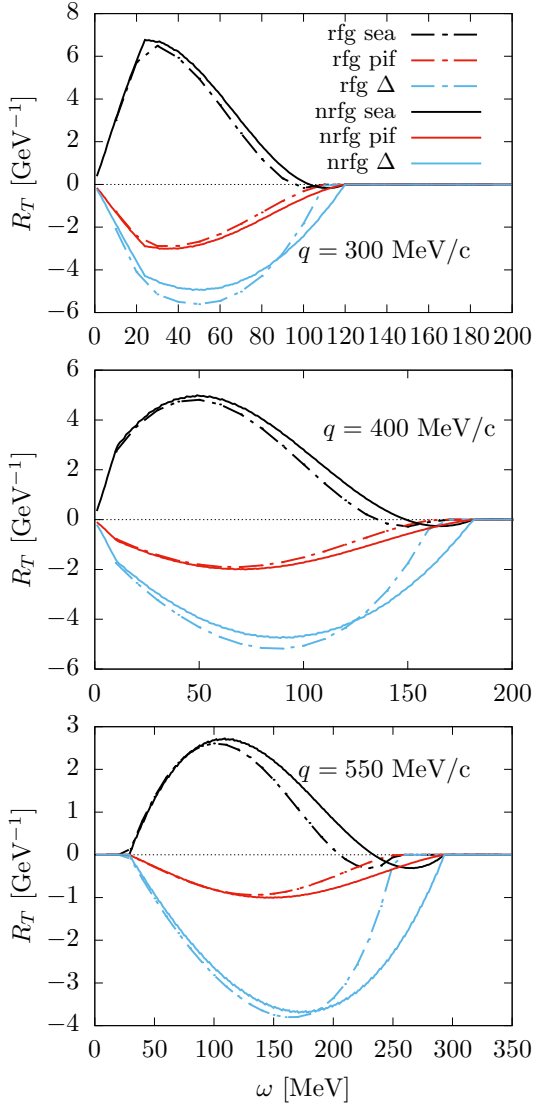


FIG. 4: Interference between one-body and two-body currents in the transverse response, separated into seagull, pion-in-flight, and Δ currents. We compare the non-relativistic Fermi Gas (nrfg) with the Relativistic Fermi Gas (rfg) for three values of the momentum transfer in the C12 nucleus. The Fermi momentum is $k_F = 225$ MeV/c. Diagrams for the 1p1h MEC matrix elements

For ^{12}C , the initial states include nucleons in the occupied shells $1s_{1/2}$ and $1p_{3/2}$. More details can be found in Refs. [38, 39]. Note that there is a typographic error in Ref. [38] regarding the relative sign between the central and spin-orbit potentials. This is merely a mistake in the written formula and does not affect the results. The energy of the $1p_{3/2}$ state is lower than that of the $1p_{1/2}$ state because the spin-orbit potential is negative for the $1p_{3/2}$ state and positive for the $1p_{1/2}$ state.

The mean-field approach accounts for some effects of the final-state interaction (FSI) in the response functions. Additionally, unlike the Fermi gas model, it incorporates

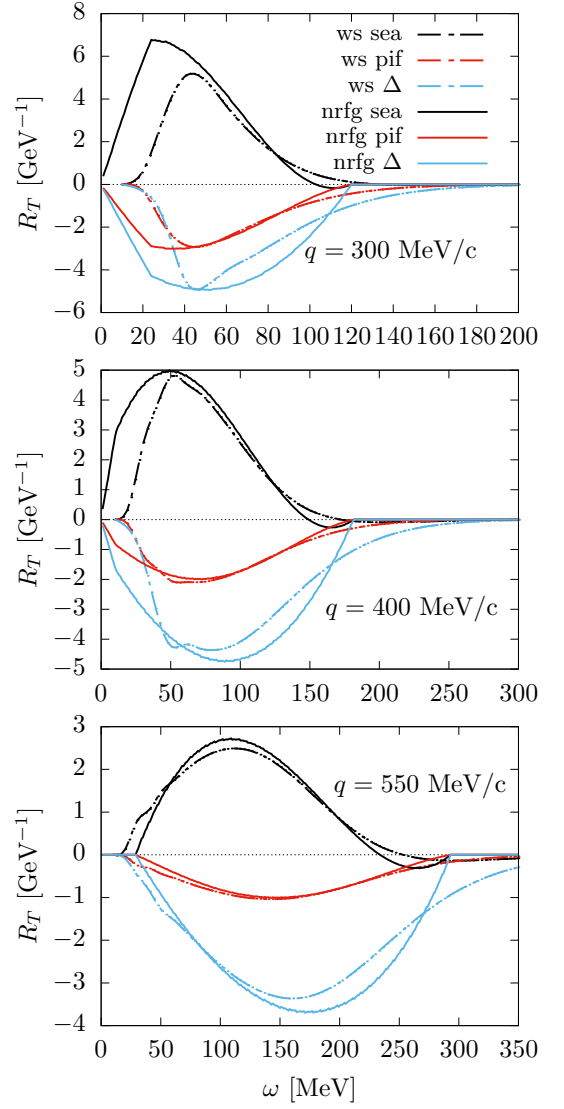


FIG. 5: The same as Fig. 4, comparing between two models: the mean field with Woods-Saxon potential (ws) and the non-relativistic Fermi Gas (nrfg) for different values of momentum transfer q with $k_F = 225$ MeV/c.

TABLE I: Parameters of the Woods-Saxon potential used in this work for the nucleus ^{12}C .

	V_0 [MeV]	V_{is} [MeV]	a [fm]	R [fm]
protons	62	3.2	0.57	2.86
neutrons	60	3.15	0.57	2.86

finite-size effects along with surface effects of the nucleus. In Fig. 5 we observe some differences between the WS model and the Fermi gas, particularly at low momentum transfer and low energy, where Pauli blocking affects the Fermi gas more significantly. The WS response shows a slight tail extending to higher energies, unlike the Fermi gas. However, at $q = 550$ MeV/c, the two models become more similar, except for the high-energy tail seen

in the WS model. A possible explanation for this similarity at intermediate momentum is that the wavelength of the exchanged photon is small compared to both the nuclear surface and the extent of the nucleon orbits or wave functions in the occupied shells.

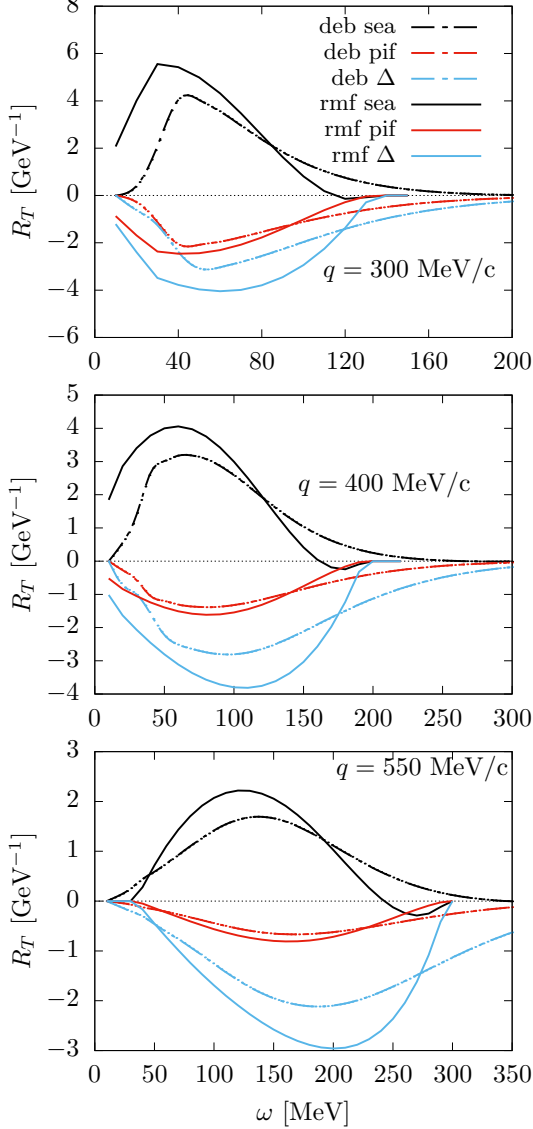


FIG. 6: The same as Fig. 4. Results are compared between two models: the relativistic mean field with DEB potential (deb) and the relativistic mean field of nuclear matter (rmf) with effective mass $M^* = 0.8$, for different values of momentum transfer q .

C. Relativistic mean field

In fig. 6 we present the interference responses for two relativistic mean field models: the Dirac-equation based (DEB) model and the relativistic mean field of nuclear matter with effective mass.

In the RMF model nucleons move in the presence of

scalar $U_S(\mathbf{r})$ and vector $U_V(\mathbf{r})$ potentials, and satisfy a Dirac-like equation for the four-component nucleon wave function $\Psi(\mathbf{r})$:

$$[\gamma^0 (E - U_V(\mathbf{r})) - \boldsymbol{\gamma} \cdot \mathbf{p} - (M + U_S(\mathbf{r}))] \Psi(\mathbf{r}) = 0. \quad (111)$$

where Ψ has up and down components

$$\Psi(\mathbf{r}) = \begin{pmatrix} \psi_u(\mathbf{r}) \\ \psi_d(\mathbf{r}) \end{pmatrix}. \quad (112)$$

The DEB potential is obtained by rewriting the Dirac equation (111) as a Klein-Gordon equation for the upper component of the wave function. In this reduction, the upper component is written in the form

$$\Psi_u(\mathbf{r}) = A^{1/2}(r, E) \phi(\mathbf{r}), \quad (113)$$

where E is the energy in the final state and $A(r, E)$ is the Darwin term

$$A(r, E) = 1 + \frac{U_S(r) - U_V(r)}{E + M}. \quad (114)$$

With this definition the function $\phi(\mathbf{r})$ verifies the equation

$$\left[-\frac{1}{2m_N} \nabla^2 + U_{DEB}(r, E) \right] \phi(\mathbf{r}) = \frac{E^2 - m_N^2}{2m_N} \phi(\mathbf{r}). \quad (115)$$

The DEB potential is given by [60, 61]

$$V_{DEB} = V_C + V_{so} \boldsymbol{\sigma} \cdot \mathbf{l} + V_D + V_{coul} \quad (116)$$

where the central, spin-orbit and Darwin potentials are given by

$$\begin{aligned} V_C(r, E) &= 2m_N U_S(r) + 2E U_V(r) + U_S(r)^2 - U_V(r)^2 \\ V_{so}(r, E) &= -\frac{1}{rA} \frac{\partial A}{\partial r} \\ V_D(r, E) &= \frac{3}{4A^2} \left(\frac{\partial A}{\partial r} \right)^2 - \frac{1}{rA} \frac{\partial A}{\partial r} - \frac{1}{2A} \frac{\partial^2 A}{\partial r^2}, \end{aligned}$$

and V_{coul} is the Coulomb potential of a homogeneously charged sphere with nuclear radius R .

In Fig. 6 we present the results of the interference 1b2b transverse response using the DEB potential within the semi-relativistic model of Refs. [65, 66]. It is observed that the contribution from the Delta current is negative, as is the contribution from the pion-in-flight current. Consequently, this model verifies the low momentum theorems.

In the same figure 6, the results using the DEB potential are compared with those obtained from the RMF of nuclear matter [41]. In this model, the scalar and vector potentials are constant, making it similar to the RFG but with the nucleon mass replaced by an effective mass $m_N^* = m_N + U_S$ and the energy increased by a constant vector energy $E_V = U_V$. For the ^{12}C case shown in Fig. 6, the values used are $m_N^* = 0.8 m_N$ and $E_V = 141$ MeV.

More details of the RMF nuclear matter model with MEC can be found in Refs. [41, 62]. As seen in Fig. 6, both the DEB model and the RMF model with effective mass yield qualitatively similar results, with the peaks of the interference responses largely coinciding. This similarity arises because both models incorporate final-state interaction effects. However, the absolute values obtained with the DEB model are smaller. This is a consequence of the fact that, in the DEB model, the effective mass depends on r , leading to responses that exhibit a tail extending much further than those in the shell model or nuclear matter. Essentially, it appears as if the strength is spread over a wider energy interval. In any case, it is remarkable that the low momentum theorems remain verified in the models presented in Fig. 6: the 1b- Δ interference is negative and the 1b-pionic one is negative.

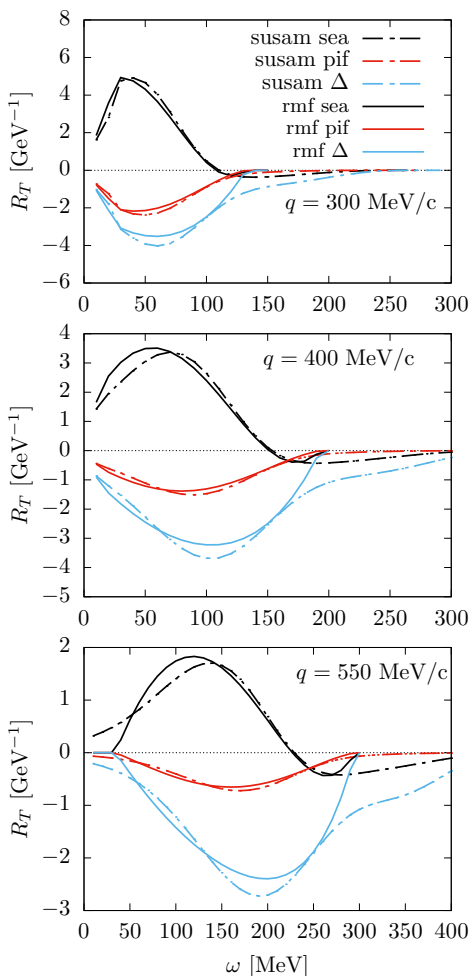


FIG. 7: The same as Fig. 4. Results are compared between two models: the superscaling model (susam) with relativistic effective mass and the relativistic mean field of nuclear matter (rmf) with effective mass $M^* = 0.8$, for different values of momentum transfer q .

D. SuSAM* model

In Fig. 7, we compare the RMF of nuclear matter with the superscaling model with effective mass (SuSAM*) as described in Ref. [41]. The SuSAM* model is an extension of the superscaling (SuSA) model presented in Ref. [63] and employs a phenomenological scaling function fitted to the quasielastic cross section data. In this approach, the cross section is approximated via factorization as the product of the phenomenological scaling function and a single-nucleon cross section, which is conveniently derived from the RMF equations of nuclear matter with effective mass, allowing for a unified description of the data with a single scaling function. Recently, the model was further refined to improve the single-nucleon prefactor by defining it as an average value of the nucleon response in the Fermi gas. This new definition enables the extension of the average response into the high-momentum region, beyond the conventional Fermi momentum, by replacing the Fermi gas momentum distribution by a smeared distribution effectively including a gradual rather than abrupt transition of the nucleon momentum distribution at the Fermi surface [64]. Instead of a sharp cutoff at the Fermi momentum, the Fermi surface is diffused over a range of momenta.

This smeared momentum distribution allows for the definition of a positive-definite averaged single-nucleon cross section, replacing the simple extrapolation of the Fermi gas average which loses its meaning outside the kinematically allowed range of the Fermi gas. Moreover, this novel procedure enabled the extension of the model in Ref. [41] to include MEC within the SuSAM* formalism by using the same smeared momentum distribution. The results of the SuSAM* model for the 1b-MEC interference are compared in Fig. 7 with those of the RMF model with effective mass. As shown in the figure, the scaling model produces responses similar to the RMF; however, the responses in the scaling model extend beyond the interval permitted by the Fermi gas. In any case, the model continues to verify the low momentum theorems.

E. Strong form factor and relativistic effects

In Fig. 8, we show the effect of including the πNN and $\pi N\Delta$ form factors. In our non-relativistic Fermi gas equations and in the low- q theorems, we have omitted these form factors for simplicity. These form factors are multiplicative factors that would be included inside the internal integrals over the intermediate nucleon momentum \mathbf{k} . Their inclusion does not affect the low momentum theorems since these form factors are positive and do not alter the sign of the interference. Moreover, in the non-relativistic calculation, some integrals can be evaluated analytically without the form factors, which further simplifies the computation. Given that we are considering small momentum transfers, the effect of the form factors

is minimal, as demonstrated in Fig. 8, where the relativistic Fermi gas results are compared with and without the strong form factor. As the form factor is less than one, the inclusion produces a reduction of the maximum in absolute value.

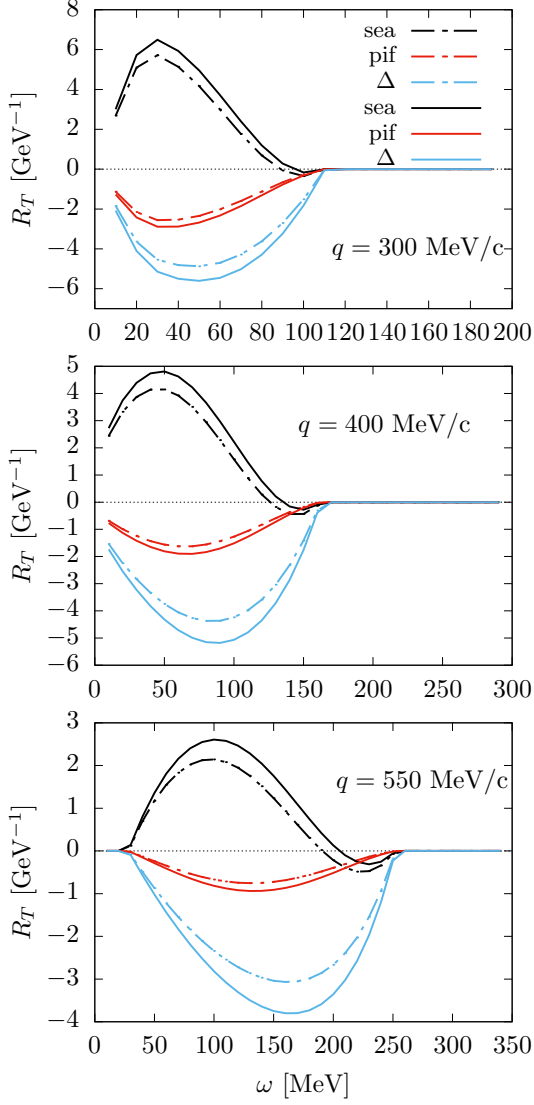


FIG. 8: The same as Fig. 4 but calculated with RFG, with and without the strong πNN form factor. The dashed line represents the results with the form factor, while the solid line represents the results without it.

The relativistic Fermi gas can be compared with the semirelativistic Fermi gas model (SRFG) developed in [40]. The SRFG model starts from the non-relativistic Fermi gas, incorporating relativistic kinematics and replacing the non-relativistic current with a semirelativistic expansion in powers of the initial nucleon momentum divided by the nucleon mass (\hbar/m), while preserving the exact dependence on the final momentum. This approach was extended to include MEC [34] and also applied to the Delta current, although in the latter case the

semirelativistic correction is not exact due to the use of a static Delta propagator. The semirelativistic current is obtained from the relativistic one by multiplying by a factor $1/\sqrt{1+\tau}$. In Fig. 9, the SRFG model is compared with the exact RFG for the interference between the MEC and the one-body current. For the seagull and pionic contributions, the SRFG model agrees very well with the relativistic one. However, for the Delta contribution, the approximation is less accurate because the static Delta propagator limits the effectiveness of the semirelativistic factor.

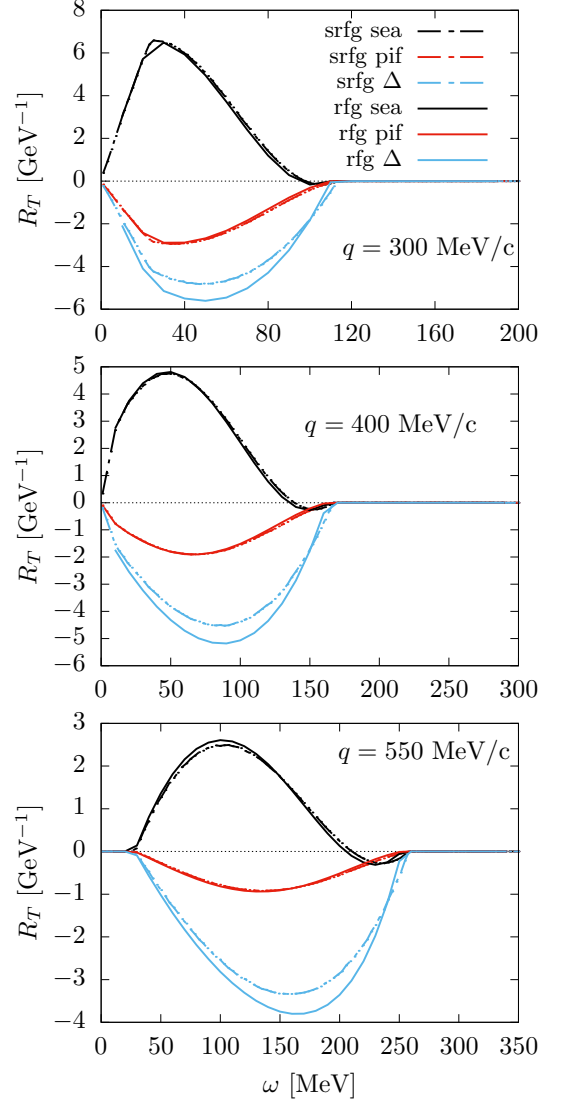


FIG. 9: The same as Fig. 4 but showing two models: relativistic Fermi gas (rfg) and semirelativistic Fermi gas (srfg). The comparison illustrates the differences between the relativistic and semirelativistic approaches in the transverse response, for different values of q .

In addition, the semirelativistic model was extended to be applied in conjunction with the Woods-Saxon mean field model [65]. This extended model can be directly

compared with the DEB model. In fact, the DEB model also incorporates semirelativistic MEC currents, but these currents are further modified because the pion propagator in the DEB model is made dynamic by including the pion energy as the difference in energy between the nuclear states of the mean field model. The comparison between these two models, DEB and SRWS, as shown in Fig. 10, reveals significant differences in both the width and the height of the interference response peak. Specifically, the DEB model extends to higher energies and exhibits a broader peak, which is attributed to the fact that the DEB potential is much stronger than the Woods-Saxon potential.

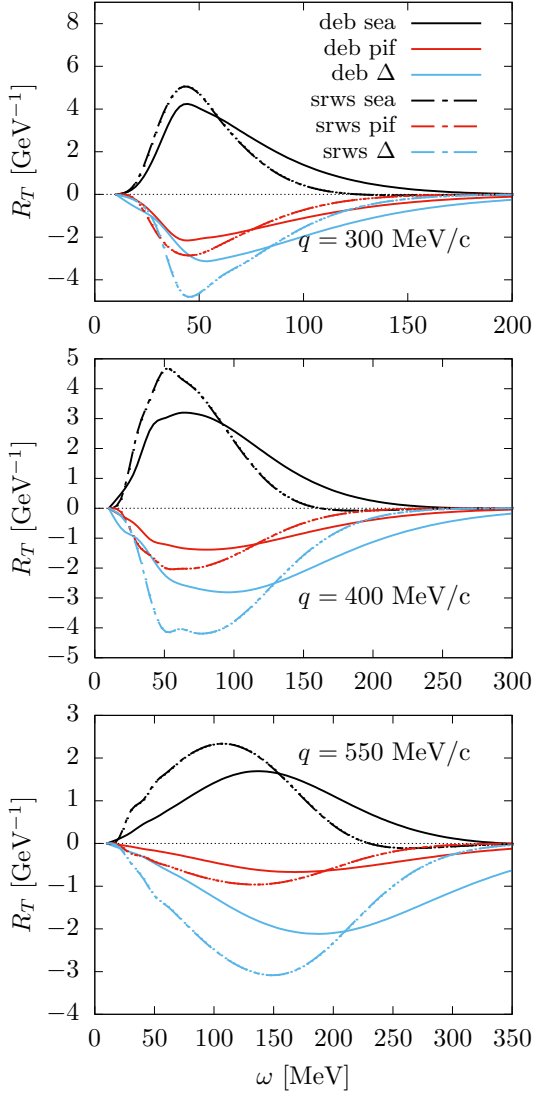


FIG. 10: The same as Fig. 4, but now comparing the models: relativistic mean field with DEB potential (deb) and semi-relativistic mean field with Woods-Saxon potential (srws) for different values of momentum transfer q .

F. Plane wave approximation

In the shell model with a Woods-Saxon potential, the plane wave approximation (PWA) assumes that the final nucleon with momentum \mathbf{p} is described by a plane wave, meaning it is a solution of the Schrödinger equation without final-state interactions. Note that in PWA the sum over hole states, h in Eq. (3) refers to a sum over occupied states in the shell model, just as the sum over spectator states k in Eq. (7) also corresponds to occupied Woods-Saxon states. Therefore, in this approach, the plane wave approximation is applied only to the final outgoing particle state, while the initial state nucleons remain described by the bound shell model wave functions.

Results using this model are presented in Fig. 11, where they are compared with the Woods-Saxon mean-field calculations for the 1b2b interference responses. The observed effect is similar to that seen in the 1b response within the Plane Wave Impulse Approximation (PWIA) [66]. The impact of final-state interactions appears as a shift in the response. This shift can be understood as a consequence of the energy imbalance between the initial and final states. In the initial state, the nucleon has both kinetic and potential energy, whereas in the final state, only kinetic energy remains, since the potential is neglected. This energy mismatch propagates to the energy-conserving delta function, altering the position of the response peak.

The shift in the response function can be qualitatively understood using a back-of-the-envelope estimate. First we assume that the matrix element of the current in PWA is approximately equal to the matrix element in the Woods-Saxon model, $\langle J^\mu \rangle_{PW} \simeq \langle J^\mu \rangle_{WS}$. Second, we approximate the potential energy of the final-state nucleon as a constant, $V_p \simeq -V < 0$. Thus, the total energy of the outgoing particle can be written as the sum of its kinetic and potential energy: $\epsilon_p = t_p - V$. Using this, the transverse response function in PWA can be expressed as

$$\begin{aligned}
 R_{PW}^T(q, \omega) &= \sum_{ph} |\langle J_T \rangle_{PW}|^2 \delta(t_p - \epsilon_h - \omega) \\
 &\simeq \sum_{ph} |\langle J_T \rangle_{WS}|^2 \delta(\epsilon_p + V - \epsilon_h - \omega) \\
 &= R_{WS}^T(q, \omega - V).
 \end{aligned} \tag{117}$$

This expression shows that the response function is effectively shifted due to the neglect of the potential in the final state.

From Fig. 11, we observe again that the low-momentum theorem for the 1b-MEC interference response remains valid in both the plane-wave approximation and the Woods-Saxon potential.

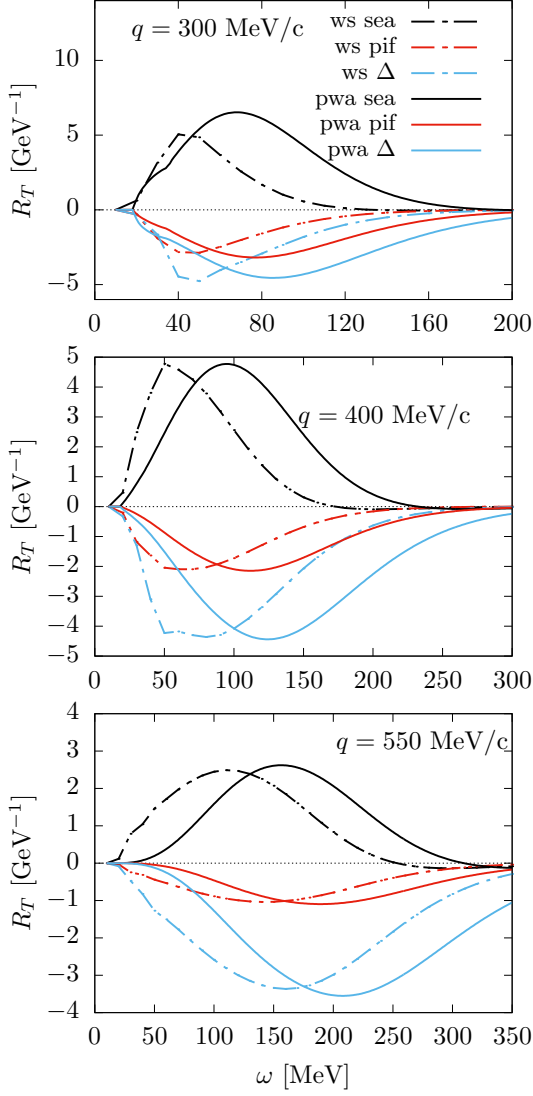


FIG. 11: The same as Fig. 4, but now comparing the models: mean field with Woods-Saxon potential (ws) and mean field in plane-wave approximation for the final state (pwa) for different values of momentum transfer q .

G. Spectral function model

In this subsection, we present results using the spectral function (SF) model, which employs the one-hole spectral function, $S(\mathbf{p}, E)$, that depends on the missing momentum and missing energy. In the SF model, the transverse response is computed assuming factorization of the single-nucleon response and the one-hole spectral function for one-particle emission.

$$R_T(q, \omega) = \int d^3p w_T(\mathbf{p}, \mathbf{p} - \mathbf{q}) S(\mathbf{p} - \mathbf{q}, \omega - T_p) \quad (118)$$

where the single nucleon response is $w^T = w^{11} + w^{22}$, while $w^{\mu\mu}$ is defined in Eq. (16).

Unlike the single-particle model that assumes holes

with definite energy, the SF approach accounts for a continuous distribution of hole energies. It provides the probability that the system contains a hole state with momentum $\mathbf{h} = \mathbf{p} - \mathbf{q}$ and a missing energy $E = \omega - T_p$, where $T_p = \mathbf{p}^2/(2m_N)$. The basic theory of the SF approach to QE electron scattering is summarized in Appendix F.

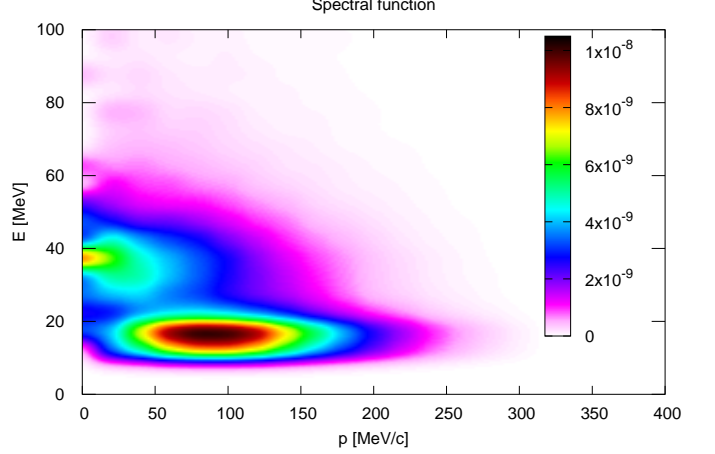


FIG. 12: Spectral function of ^{12}C in units of $\text{MeV}^{-4}c^3$

We use the spectral function, $S(p, E)$, for ^{12}C taken from Ref. [67] for both protons and neutrons, as shown in Fig. 12. This spectral function exhibits peaks around $E \simeq 19$ MeV and $E \simeq 39$ MeV as a function of energy. These values are close to the binding energies of the $1p_{3/2}$ and $1s_{1/2}$ shells in the extreme shell model, where the nuclear wave function is described by a Slater determinant.

In the shell model, the spectral function is given by

$$S(p, E) = \sum_{nlj} (2j + 1) |\tilde{R}_{nlj}(p)|^2 \delta(E + \epsilon_{nlj}) \quad (119)$$

where the sum runs over occupied shells, and $\tilde{R}_{nlj}(h)$ are the shell radial wave functions in momentum space, with single-particle energy ϵ_{nlj} . In the more realistic spectral function of Fig. 12, the energy dependence is smeared around the shell binding energies, resulting in a continuous energy distribution instead of discrete shell levels.

In Fig. 13, we show the proton momentum distribution $n(p)$ obtained by integrating the spectral function over the missing energy. This distribution is compared with the constant momentum distribution of the Fermi gas model. Additionally, we present the radial momentum distribution, $4\pi n(p)p^2$, which highlights the probability density of nucleons as a function of momentum. The missing energy distribution, obtained by integrating the spectral function over momentum, is also displayed. The normalization follows $\int d^3p n(p) = 6$ for ^{12}C , reflecting that the proton and neutron distributions are identical in this model.

It is worth noting that the response function in the SF model, Eq. (118), is expressed as an integral over the final nucleon momentum p . To evaluate this integral, it

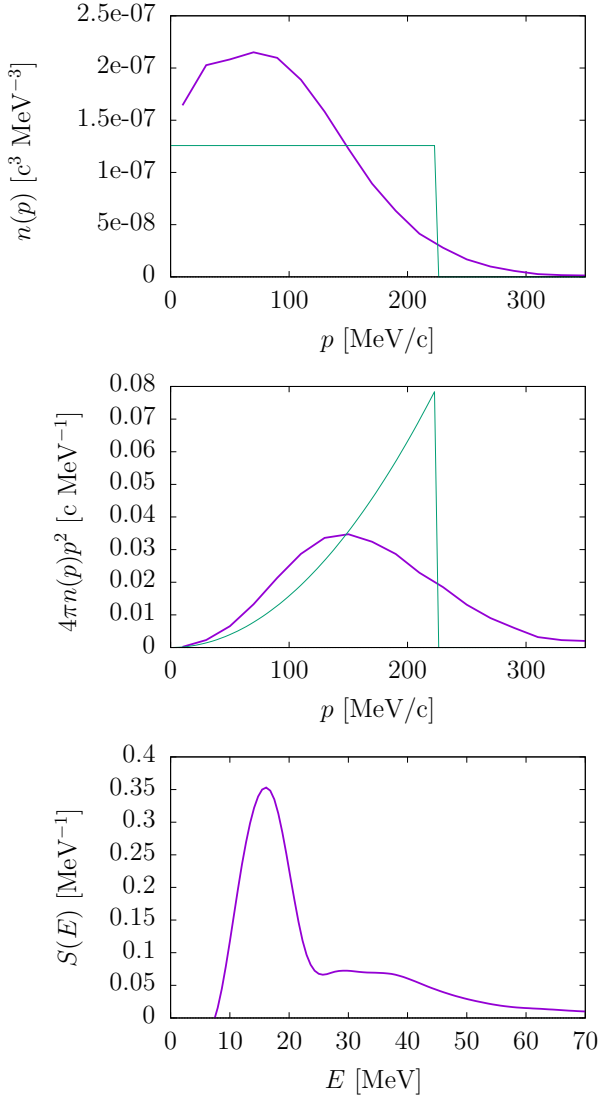


FIG. 13: Proton momentum distribution of ^{12}C (top), radial momentum distribution (middle) and missing energy distribution (bottom), obtained from the spectral function by integration.

is convenient to first integrate over the missing energy and missing momentum. The missing energy is given by

$$E = \omega - T_p = \omega - \frac{p^2}{2m_N}. \quad (120)$$

Differentiating, we obtain $dE = -p dp/m_N$, and the volume element in spherical coordinates is

$$d^3p = m_N p dE d\Omega$$

where θ and ϕ are the nucleon emission angles. The response function can then be rewritten as

$$R_T(q, \omega) = m_N \int dE d\Omega p w_T(\mathbf{p}, \mathbf{p} - \mathbf{q}) S(\mathbf{p} - \mathbf{q}, E). \quad (121)$$

Next, we define $\mathbf{h} = \mathbf{p} - \mathbf{q}$, leading to the relation $h^2 = p^2 + q^2 - 2pq \cos \theta$, where θ is the angle between \mathbf{p} and \mathbf{q} , with \mathbf{q} chosen along the z -axis. Differentiating with respect to θ , we obtain $h dh = -pq d \cos \theta$.

Substituting this into the integral (121), we can express the transverse response as

$$R_T(q, \omega) = 2\pi \frac{m}{q} \int_0^\omega dE \int_{|p-q|}^{p+q} S(h, E) w_T(\mathbf{h} + \mathbf{q}, \mathbf{h}) dh, \quad (122)$$

where $p = \sqrt{2m_N(\omega - E)}$. Note that $E < \omega$ ensures that p is well defined. The factor 2π arises from the integration over ϕ , and the integration limits in h correspond to nucleon emission in the direction of $\pm \mathbf{q}$.

The effect of MEC is estimated by treating the spectator nucleon in Eq (7) as an on-shell plane-wave with momentum \mathbf{k} , therefore we replace the single-nucleon response by the effective single nucleon including MEC, in Eq. (16). This approximation has been done in the past in previous calculations by the Pavia group for $(e, e'p)$ reactions [68], and in recent RMF-based calculations [45, 46], where the spectator nucleon is described using an effective mass and vector energy. A similar approach to MEC was also adopted in the spectral function model of Ref. [47]. Thus the transverse response is evaluated using the effective single nucleon, Eq. (16), which includes the MEC contribution, effectively decoupling it from the spectral function.

In the spectral function model, the interference MEC-OB responses are presented in Fig. 14 for the separate contributions from the seagull, pion-in-flight, and Δ currents. The figure compares the SF results with those obtained using the PW model from the previous subsection. Both models yield quite similar results. This similarity arises from the fact that both models assume plane waves for the final-state nucleon. In the PW model, the response is obtained by summing the contributions from each shell separately, while in the SF model, the shell contributions are smeared according to the spectral function's energy distribution. However, this smearing effect is barely noticeable in the inclusive response, as the information about the hole energy is lost. Furthermore, the agreement between the SF and PWIA models reinforces the validity of the approximation that treats the spectator nucleon as a plane wave. While this approximation is not explicitly made in the PW model, it is assumed in the SF model. In conclusion, the SF model, as applied here, fully adheres to the low-momentum theorem, consistent with all the models analyzed in this work.

H. Total interference response

To conclude the results section, we present a comprehensive comparison of most of the models discussed in this paper to assess the overall impact of MEC and the theoretical uncertainties. In Fig. 15, we display the total 1b-MEC interference for a selection of seven models.

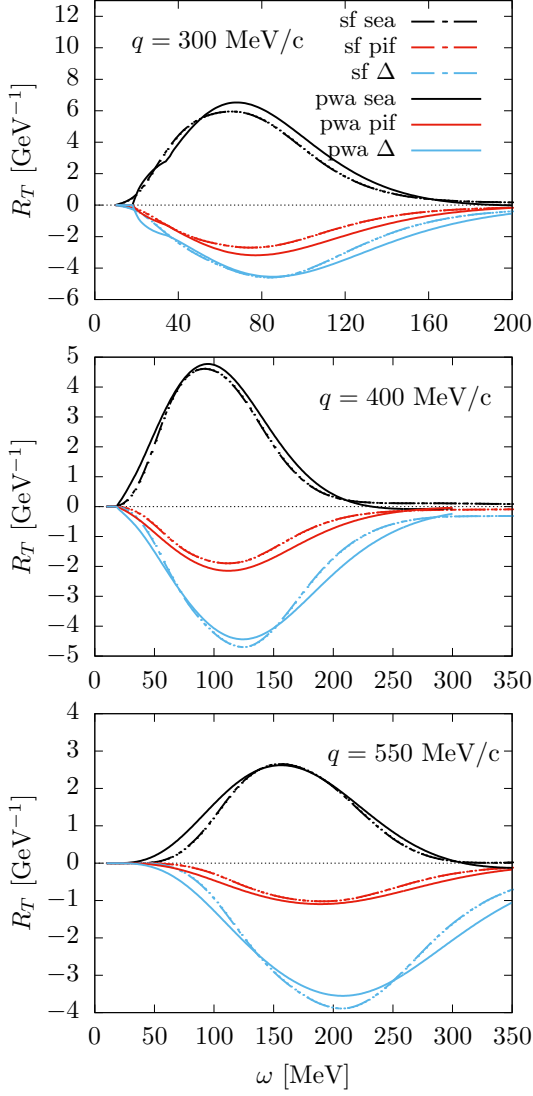


FIG. 14: The same as Fig. 4, but now comparing the models: spectral function (sf) and mean field with plane-wave approximation (pwa) for different values of momentum transfer q .

All models consistently predict a negative interference, although there are significant quantitative differences in the position of the peak and the width of the distribution. Despite these variations, the overall magnitude remains comparable, with differences up to a factor of two. Importantly, the key takeaway from this comparison — and one of the main objectives of this work — is that the low-momentum theorem holds across all models analyzed. This explains why none of the models exhibit a qualitative deviation, such as a sign change in the interference term.

To end we list here the models considered in this paper:

1. Non relativistic Fermi gas (nrfg)
2. Relativistic Fermi gas (rfg)
3. Mean field with Woods-Saxon potential (ws)

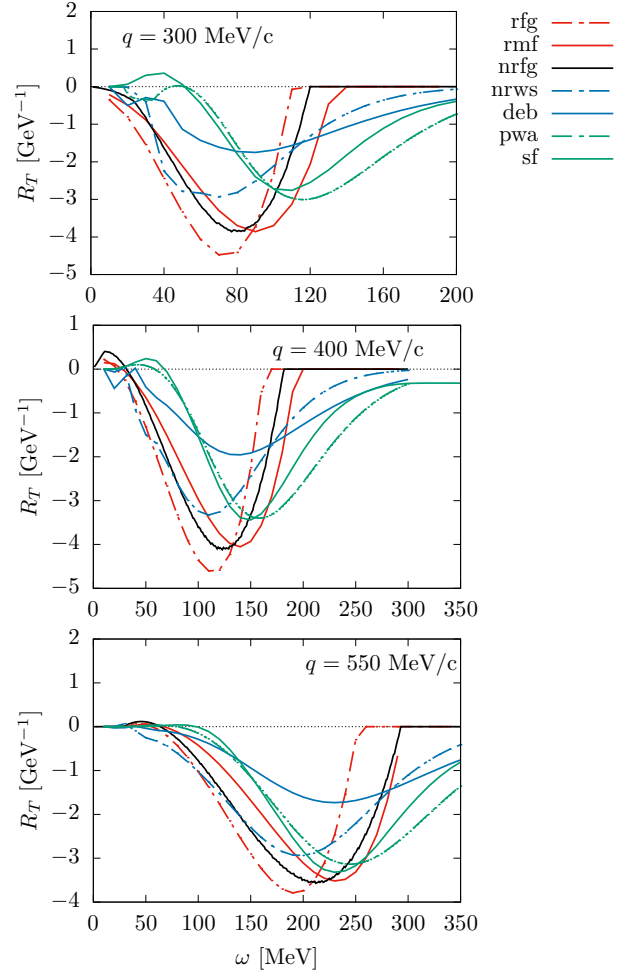


FIG. 15: Total interference OB-MEC compared across all different models considered in this work for all values of q . The πNN form factor is not included.

4. Mean field with Dirac-equation based potential (deb)
5. Relativistic mean field of nuclear matter with effective mass (rmf)
6. Mean field with plane wave approximation (pwa)
7. Semirelativistic mean field with Woods-Saxon (srws)
8. Semirelativistic Fermi gas (srfg)
9. Superscaling model with effective mass (susam)
10. Spectral function (sf) .

IV. CONCLUSIONS

In this work, we have conducted a detailed reexamination of the OB-MEC interference in the one-particle emission transverse response, focusing on its sign. We

systematically compared various models, obtaining qualitatively consistent results. A key aspect of our analysis was the derivation of two low-momentum theorems within the non-relativistic Fermi gas framework, ensuring full transparency and reproducibility in our approach. The theorems clearly establish that the sign of the interference of the one-body current with the pionic and Δ currents is negative in the Fermi gas model.

Our results show also that all models considered satisfy these low-momentum theorems. The common feature among these models is that they are based on independent-particle descriptions—either relativistic or non-relativistic— or extensions, such as the one-hole spectral function for one-particle emission in electron scattering. Crucially, these models do not include explicit two-body correlations beyond mean-field approximations.

Given these results, it does not seem possible to explain any enhancement in the transverse response in one-particle emission using models that do not include fundamentally different ingredients that would violate the low-momentum theorems, in contrast with the results of Refs. [45–47]. A candidate for producing such an enhancement is the inclusion of tensor correlations, as suggested by the microscopic calculation of Ref. [42]. These correlations could introduce contributions that go beyond the low-momentum theorem, thus altering the single-particle dynamics of the models analyzed here. However, no study after that of Ref. [42] has been conducted to confirm this effect. Future research along these lines is planned, aiming to include the effect of short-range correlations and high-momentum components in a two-body independent-pair approximation, solving the Bethe-Goldstone equation, as outlined in Ref. [69]. In parallel, similar studies for neutrino scattering are also in progress.

V. ACKNOWLEDGMENTS

We thank Luis Alvarez-Ruso for helpful discussions.

The work was supported by Grant No. PID2023-147072NB-I00 funded by MICIU/AEI/10.13039/501100011033 and by ERDF/EU; by Grant No. FQM-225 funded by Junta de Andalucía; by Grant NUCSYS funded by INFN; by Grant No. BARM-RILO-24-01 funded by University of Turin; by the “Planes Complementarios de I+D+i” program (Grant ASFAE/2022/022) by MICIU with funding from the European Union NextGenerationEU and Generalitat Valenciana.

Appendix A: Lagrangian

In this appendix we display the Lagrangian terms needed in order to obtain the meson-exchange currents. The πNN interaction is described using the following Lagrangian

$$\mathcal{L}_{\pi NN} = -\frac{f}{m_\pi} \bar{\Psi} \gamma^\mu \gamma_5 \boldsymbol{\tau} \cdot \partial_\mu \boldsymbol{\phi} \Psi, \quad (\text{A1})$$

where Ψ represents the nucleon isospinor, and $\boldsymbol{\phi}$ is the isospin triplet pion field $\boldsymbol{\phi} = (\phi_1, \phi_2, \phi_3)$:

$$\begin{aligned} \Psi &= \begin{pmatrix} \psi_p \\ \psi_n \end{pmatrix}, & \boldsymbol{\tau} \cdot \boldsymbol{\phi} &= \frac{\tau_+ \phi + \tau_- \phi^\dagger}{\sqrt{2}} + \tau_3 \phi_3, \\ \tau_\pm &\equiv \tau_1 \pm i\tau_2, & \phi &\equiv \frac{\phi_1 - i\phi_2}{\sqrt{2}}. \end{aligned} \quad (\text{A2})$$

The electromagnetic interactions with the photon field A_μ are defined as

$$\mathcal{L}_{\gamma\pi\pi} = -ieA_\mu (\phi^\dagger \partial^\mu \phi - \phi \partial^\mu \phi^\dagger), \quad (\text{A3})$$

$$\mathcal{L}_{\gamma NN\pi} = -ieA_\mu \frac{f}{m_\pi} \bar{\Psi} \gamma^\mu \gamma_5 \frac{\tau_+ \phi - \tau_- \phi^\dagger}{\sqrt{2}} \Psi, \quad (\text{A4})$$

with $e > 0$ the elementary electric charge. The Δ interactions are described using the following Lagrangians

$$\mathcal{L}_{\pi N\Delta} = \frac{f^*}{m_\pi} \bar{\psi}_\mu \partial^\mu \boldsymbol{\phi} \cdot \mathbf{T}^\dagger \Psi + h.c., \quad (\text{A5})$$

$$\mathcal{L}_{\gamma N\Delta} = ie \frac{G}{2m_N} \sqrt{\frac{3}{2}} \bar{\psi}_\mu \gamma_\nu \gamma_5 T_3^\dagger \Psi F^{\mu\nu} + h.c., \quad (\text{A6})$$

where ψ_μ is the 3/2 spin Rarita-Schwinger Δ field, $G = 2C_3^V(Q^2 = 0)$, with C_3^V defined in Eq. (36), and $F^{\mu\nu} = \partial^\mu A^\nu - \partial^\nu A^\mu$ the standard electromagnetic tensor. The $3/2 \rightarrow 1/2$ isospin transition operator \mathbf{T} definition is here reported:

$$\begin{aligned} T_1 &= \frac{1}{\sqrt{6}} \begin{pmatrix} -\sqrt{3} & 0 & 1 & 0 \\ 0 & -1 & 0 & \sqrt{3} \end{pmatrix} \\ T_2 &= -\frac{i}{\sqrt{6}} \begin{pmatrix} \sqrt{3} & 0 & 1 & 0 \\ 0 & 1 & 0 & \sqrt{3} \end{pmatrix} \\ T_3 &= \sqrt{\frac{2}{3}} \begin{pmatrix} 0 & 1 & 0 & 0 \\ 0 & 0 & 1 & 0 \end{pmatrix}. \end{aligned} \quad (\text{A7})$$

Appendix B: Non relativistic reduction of the Δ current

Here we perform the non relativistic reduction of the four-vectors A^μ , and B^μ , Eqs. (60,61), appearing in the

Δ -current. Using the definition of the $\gamma N\Delta$ vertex, Eq. (35) we have

$$A^\mu = \bar{u}(1') k_2^\alpha G_{\alpha\beta} (p_1 + Q) \frac{C_3^V}{m_N} (g^{\beta\mu} \mathcal{Q} - Q^\beta \gamma^\mu) \gamma_5 u(1) \quad (\text{B1})$$

$$B^\mu = \bar{u}(1') k_2^\beta \frac{C_3^V}{m_N} \gamma_5 (g^{\alpha\mu} \mathcal{Q} - Q^\alpha \gamma^\mu) G_{\alpha\beta} (p_1' - Q) u(1). \quad (\text{B2})$$

In the last equation we have permuted the γ_5 matrix, which introduces a minus sign that cancels with the negative sign from $-Q$. We only need to perform the non-relativistic reduction of the spatial components ($\mu = i$) of the Δ current, since we are computing the transverse response. In the non relativistic limit we neglect the time components of k^μ and Q^μ , i. e.

$$k_2^\mu \simeq (0, \mathbf{k}_2), \quad Q^\mu \simeq (0, \mathbf{q}). \quad (\text{B3})$$

Then for the A^i components we have

$$\begin{aligned} A^i &\simeq \bar{u}(1') k_2^k G_{kj} \frac{C_3^V}{m_N} (g^{ji} \mathcal{Q} - Q^j \gamma^i) \gamma_5 u(1), \\ &= \bar{u}(1') k_2^k G_{kj} (p_1 + Q) \Gamma^{ji}(Q) u(1). \end{aligned} \quad (\text{B4})$$

Hence at leading order in the non-relativistic limit, only the spatial components of the Δ propagator G_{kj} and the vertex Γ_{ji} contribute, while the time components are suppressed. Analogously, we obtain a similar result for the backward vector components B^i ,

$$\begin{aligned} B^i &\simeq \bar{u}(1') k_2^k \frac{C_3^V}{m_N} \gamma_5 (g^{ji} \mathcal{Q} - Q^j \gamma^i) G_{jk} u(1), \\ &= \bar{u}(1') k_2^k \Gamma^{ji}(-Q) G_{jk} (p_1' - Q) u(1). \end{aligned} \quad (\text{B5})$$

Furthermore, the procedure we follow to compute the non-relativistic reduction of a product of matrix operators is to perform the reduction on each operator separately. This approach is valid at leading order.

a. Δ propagator

We begin with the Δ propagator. In the static limit, with $p^\mu + Q^\mu \simeq (p^0, 0) = (m_N, 0)$, and neglecting the lower components we have

$$\frac{\not{p} + m_\Delta}{p^2 - m_\Delta^2} \rightarrow \frac{p_0 + m_\Delta}{p_0^2 - m_\Delta^2} = \frac{1}{m_N - m_\Delta}. \quad (\text{B6})$$

Then the Δ propagator is written as

$$\begin{aligned} G_{ij} &\simeq -\frac{1}{m_N - m_\Delta} (g_{ij} - \frac{1}{3} \gamma_i \gamma_j) \\ &\simeq -\frac{1}{m_N - m_\Delta} (-\delta_{ij} + \frac{1}{3} \sigma_i \sigma_j) \\ &= \frac{1}{m_N - m_\Delta} \left(\frac{2}{3} \delta_{ij} - i \frac{1}{3} \epsilon_{ijk} \sigma_k \right) \end{aligned} \quad (\text{B7})$$

where we have used the property

$$\sigma_i \sigma_j = i \epsilon_{ijk} \sigma_k \quad (\text{B8})$$

and ϵ_{ijk} is the Levi-Civita tensor.

b. $\gamma N \Delta$ vertex

To obtain the non-relativistic reduction of the vertex

$$\Gamma^{ji}(Q) = \frac{C_3^V}{m_N} (g^{ji} \not{Q} - Q^j \gamma^i) \gamma_5, \quad (\text{B9})$$

in the low energy limit, we have $Q^\mu \simeq (0, q^i)$. Then

$$\begin{aligned} (g^{ji} \not{Q} - Q^j \gamma^i) \gamma_5 &\simeq \delta_{ji} q^k \gamma^k \gamma_5 - q^j \gamma^i \gamma_5 \\ &\simeq \delta_{ji} q^k \sigma_k - q^j \sigma_i \\ &= q^k \sigma_l (\delta_{ij} \delta_{kl} - \delta_{il} \delta_{kj}). \end{aligned} \quad (\text{B10})$$

This expression can be rewritten using the contraction of two Levi-Civita tensors

$$\epsilon_{ikm} \epsilon_{jlm} = \delta_{ij} \delta_{kl} - \delta_{il} \delta_{kj}. \quad (\text{B11})$$

Therefore we have the non relativistic reduction

$$\Gamma^{ji}(Q) \simeq \frac{C_3^V}{m_N} (\epsilon_{ikm} q^k) (\epsilon_{jlm} \sigma_l). \quad (\text{B12})$$

c. Forward vector A^i

From Eq. (B4) we have (we do not write the spinors, just the spin operators):

$$\begin{aligned} A^i &\simeq k_2^k G_{kj} \frac{C_3^V}{m_N} (\epsilon_{inm} q^n) (\epsilon_{jlm} \sigma_l) \\ &= \frac{C_3^V}{m_N} \epsilon_{inm} q^n a_m, \end{aligned} \quad (\text{B13})$$

where we have defined the vector

$$a_m \equiv \epsilon_{jlm} k_2^k G_{kj} \sigma_l. \quad (\text{B14})$$

(note that G_{kj} and σ_l do not commute). Therefore we can write, in vector form

$$\mathbf{A} \simeq \frac{C_3^V}{m_N} (\mathbf{q} \times \mathbf{a}). \quad (\text{B15})$$

Hence \mathbf{A} is purely transverse.

d. Backward vector B^i

Similarly, from Eq. (B5),

$$\begin{aligned} B^i &\simeq -k_2^k \frac{C_3^V}{m_N} (\epsilon_{inm} q^n) (\epsilon_{jlm} \sigma_l) G_{jk} \\ &= \frac{C_3^V}{m_N} \epsilon_{inm} q^n b_m, \end{aligned} \quad (\text{B16})$$

where we have defined the vector

$$b_m \equiv -\epsilon_{jlm} k_2^k \sigma_l G_{jk}. \quad (\text{B17})$$

In vector form we have

$$\mathbf{B} \simeq \frac{C_3^V}{m_N} (\mathbf{q} \times \mathbf{b}). \quad (\text{B18})$$

e. Vectors a^i and b^i

Next, we perform the necessary contractions to derive the explicit expressions for the vectors \mathbf{a} and \mathbf{b} in the non relativistic limit. Using Eq. (B7) for the static Δ -propagator, we have

$$a_m \simeq \frac{\epsilon_{jlm} k_2^k}{m_N - m_\Delta} \left(\frac{2}{3} \delta_{kj} - i \frac{1}{3} \epsilon_{kjm} \sigma_n \right) \sigma_l \quad (\text{B19})$$

$$b_m \simeq \frac{-\epsilon_{jlm} k_2^k}{m_N - m_\Delta} \sigma_l \left(\frac{2}{3} \delta_{kj} - i \frac{1}{3} \epsilon_{jkm} \sigma_n \right). \quad (\text{B20})$$

Hence

$$\begin{aligned} (m_N - m_\Delta) a_m &\simeq \frac{2}{3} \epsilon_{jlm} k_2^j \sigma_l \\ &\quad - \frac{i}{3} k_2^k \epsilon_{kjm} \epsilon_{jlm} \sigma_n \sigma_l \end{aligned} \quad (\text{B21})$$

$$\begin{aligned} (m_N - m_\Delta) b_m &\simeq -\frac{2}{3} \epsilon_{jlm} k_2^j \sigma_l \\ &\quad + \frac{i}{3} k_2^k \epsilon_{jkm} \epsilon_{jlm} \sigma_l \sigma_n. \end{aligned} \quad (\text{B22})$$

To compute the contractions in the second summand, we employ again the property (B11) of the Levi-Civita tensor

$$\epsilon_{jnk} \epsilon_{jlm} = \delta_{nl} \delta_{km} - \delta_{nm} \delta_{kl}. \quad (\text{B23})$$

Then we have

$$\begin{aligned} k_2^k \epsilon_{kjm} \epsilon_{jlm} \sigma_n \sigma_l &= k_2^k (\delta_{nl} \delta_{km} - \delta_{nm} \delta_{kl}) \sigma_n \sigma_l \\ &= k_2^m \sigma_n \sigma_n - k_2^l \sigma_m \sigma_l \\ &= 3k_2^m - k_2^l (\delta_{ml} + i \epsilon_{mln} \sigma_n) \\ &= 2k_2^m - i \epsilon_{mln} k_2^l \sigma_n \\ &= (2\mathbf{k}_2 - i\mathbf{k}_2 \times \boldsymbol{\sigma})^m, \end{aligned} \quad (\text{B24})$$

and

$$\begin{aligned} k_2^k \epsilon_{jkn} \epsilon_{jlm} \sigma_l \sigma_n &= k_2^k (\delta_{lk} \delta_{mn} - \delta_{ln} \delta_{mk}) \sigma_l \sigma_n \\ &= k_2^l \sigma_l \sigma_m - k_2^m \sigma_l \sigma_l \\ &= -3k_2^m + k_2^l (\delta_{lm} + i \epsilon_{lmn} \sigma_n) \\ &= -2k_2^m - i \epsilon_{mln} k_2^l \sigma_n \\ &= (-2\mathbf{k}_2 - i\mathbf{k}_2 \times \boldsymbol{\sigma})^m. \end{aligned} \quad (\text{B25})$$

Then we can write in vector form \mathbf{a} and \mathbf{b} as

$$\begin{aligned} (m_N - m_\Delta)\mathbf{a} &\simeq \frac{2}{3}(\mathbf{k}_2 \times \boldsymbol{\sigma}) - \frac{i}{3}(2\mathbf{k}_2 - i\mathbf{k}_2 \times \boldsymbol{\sigma}) \\ &= -\frac{2}{3}i\mathbf{k}_2 + \frac{1}{3}\mathbf{k}_2 \times \boldsymbol{\sigma} \end{aligned} \quad (\text{B26})$$

$$\begin{aligned} (m_N - m_\Delta)\mathbf{b} &\simeq -\frac{2}{3}(\mathbf{k}_2 \times \boldsymbol{\sigma}) + \frac{i}{3}(-2\mathbf{k}_2 - i\mathbf{k}_2 \times \boldsymbol{\sigma}) \\ &= -\frac{2}{3}i\mathbf{k}_2 - \frac{1}{3}\mathbf{k}_2 \times \boldsymbol{\sigma}. \end{aligned} \quad (\text{B27})$$

Using this result in Eqs. (B15,B18) finally we find

$$\mathbf{A} \simeq \frac{C_3^V}{m_N} \frac{1}{m_N - m_\Delta} \mathbf{q} \times \left[-\frac{2}{3}i\mathbf{k}_2 + \frac{1}{3}\mathbf{k}_2 \times \boldsymbol{\sigma} \right] \quad (\text{B28})$$

$$\mathbf{B} \simeq \frac{C_3^V}{m_N} \frac{1}{m_N - m_\Delta} \mathbf{q} \times \left[-\frac{2}{3}i\mathbf{k}_2 - \frac{1}{3}\mathbf{k}_2 \times \boldsymbol{\sigma} \right] \quad (\text{B29})$$

from where Eqs. (62) and (63) follow.

Appendix C: Isospin Summations in the 1p1h MEC Matrix Element

Here we provide the sums over the isospin index t_k of the spectator nucleon appearing in the 1p1h MEC matrix element. The isospin dependence of the MEC is of the form

$$\mathbf{j} = \tau_z^{(1)}\mathbf{j}_1 + \tau_z^{(2)}\mathbf{j}_2 + i[\boldsymbol{\tau}^{(1)} \times \boldsymbol{\tau}^{(2)}]_z \mathbf{j}_3, \quad (\text{C1})$$

where $\boldsymbol{\tau}^{(1)}$ and $\boldsymbol{\tau}^{(2)}$ are isospin operators of the first and second particle, respectively. We begin by referencing the Pauli matrices, which also represent the isospin operators required.

$$\tau_1 = \begin{pmatrix} 0 & 1 \\ 1 & 0 \end{pmatrix}, \quad \tau_2 = \begin{pmatrix} 0 & -i \\ i & 0 \end{pmatrix}, \quad \tau_3 = \begin{pmatrix} 1 & 0 \\ 0 & -1 \end{pmatrix}. \quad (\text{C2})$$

These matrices act on the isospin states of nucleons, $|t\rangle$, for protons ($t = +\frac{1}{2}$) and neutrons ($t = -\frac{1}{2}$). We need the basic result

$$\begin{aligned} \tau_1|p\rangle &= |n\rangle, & \tau_1|n\rangle &= |p\rangle \\ i\tau_2|p\rangle &= -|n\rangle & i\tau_2|n\rangle &= |p\rangle. \end{aligned}$$

By expanding the vector product

$$i[\boldsymbol{\tau}^{(1)} \times \boldsymbol{\tau}^{(2)}]_z = i\tau_1^{(1)}\tau_2^{(2)} - i\tau_2^{(1)}\tau_1^{(2)}, \quad (\text{C3})$$

we obtain

$$\begin{aligned} i[\boldsymbol{\tau}^{(1)} \times \boldsymbol{\tau}^{(2)}]_z |pp\rangle &= 0, \\ i[\boldsymbol{\tau}^{(1)} \times \boldsymbol{\tau}^{(2)}]_z |nn\rangle &= 0, \\ i[\boldsymbol{\tau}^{(1)} \times \boldsymbol{\tau}^{(2)}]_z |pn\rangle &= 2|np\rangle = 4t_p|np\rangle, \\ i[\boldsymbol{\tau}^{(1)} \times \boldsymbol{\tau}^{(2)}]_z |np\rangle &= -2|pn\rangle = 4t_n|pn\rangle. \end{aligned}$$

These four equations can be written in unified form as

$$i[\boldsymbol{\tau}^{(1)} \times \boldsymbol{\tau}^{(2)}]_z |t_1 t_2\rangle = 4t_1(1 - \delta_{t_1 t_2})|t_2 t_1\rangle. \quad (\text{C4})$$

From these elementary results, we can compute the sums over t_k appearing in the direct and exchange matrix elements of the current.

a. Direct terms.

For the the direct terms we have:

$$\sum_{t_k=\pm 1/2} \langle t_p t_k | \tau_z^{(1)} | t_h t_k \rangle = \sum_{t_k} \delta_{t_p t_h} 2t_h = \delta_{t_p t_h} 4t_h, \quad (\text{C5})$$

$$\sum_{t_k} \langle t_p t_k | \tau_z^{(2)} | t_h t_k \rangle = \sum_{t_k} \delta_{t_p t_h} 2t_k = 0, \quad (\text{C6})$$

$$\begin{aligned} \sum_{t_k} \langle t_p t_k | i[\boldsymbol{\tau}^{(1)} \times \boldsymbol{\tau}^{(2)}]_z | t_h t_k \rangle &= \\ &= \sum_{t_k} \delta_{t_p t_k} \delta_{t_k t_h} 4t_k(1 - \delta_{t_p t_h}) = 0. \end{aligned} \quad (\text{C7})$$

b. Exchange terms.

For the the exchange matrix elements we have:

$$\sum_{t_k} \langle t_p t_k | \tau_z^{(1)} | t_k t_h \rangle = \sum_{t_k} \delta_{t_p t_k} \delta_{t_k t_h} 2t_k = \delta_{t_p t_h} 2t_h, \quad (\text{C8})$$

$$\sum_{t_k} \langle t_p t_k | \tau_z^{(2)} | t_k t_h \rangle = \sum_{t_k} \delta_{t_p t_k} \delta_{t_k t_h} 2t_h = \delta_{t_p t_h} 2t_h, \quad (\text{C9})$$

$$\begin{aligned} \sum_{t_k} \langle t_p t_k | i[\boldsymbol{\tau}^{(1)} \times \boldsymbol{\tau}^{(2)}]_z | t_k t_h \rangle &= \\ &= \sum_{t_k} \langle t_p t_k | 4t_k(1 - \delta_{t_k t_h}) | t_k t_h \rangle \\ &= \sum_{t_k} \delta_{t_p t_h} 4t_k(1 - \delta_{t_k t_h}) = -\delta_{t_p t_h} 4t_h. \end{aligned} \quad (\text{C10})$$

c. Null Δ diagrams.

Next, we will demonstrate that diagrams (e) and (f) corresponding to the Δ current are zero after summing over isospin. To achieve this, we must use the original form of the isospin operators, Eqs. (32,33). The forward current involves the operators $U_F(1,2)$ and $U_F(2,1)$, while the backward current contains the isospin operators $U_B(1,2)$ and $U_B(2,1)$. By carefully analyzing these operators, we can show that the specific contributions from diagrams (e) and (f) cancel out, leading to a net zero result for each. First, from property (67) we can write the following products

$$T_1 T_3^\dagger = \frac{i}{3} \tau_2 \quad T_2 T_3^\dagger = -\frac{i}{3} \tau_1 \quad (\text{C11})$$

$$T_3 T_1^\dagger = -\frac{i}{3} \tau_2 \quad T_3 T_2^\dagger = \frac{i}{3} \tau_1 \quad (\text{C12})$$

$$T_3 T_3^\dagger = \frac{2}{3}. \quad (\text{C13})$$

From here, using $\tau_1\tau_2 = -\tau_2\tau_1 = i\tau_3$, we have

$$\begin{aligned}\sum_i \tau_i T_i T_3^\dagger &= \tau_1 T_1 T_3^\dagger + \tau_2 T_2 T_3^\dagger + \tau_3 T_3 T_3^\dagger \\ &= \frac{i}{3}\tau_1\tau_2 - \frac{i}{3}\tau_2\tau_1 + \frac{2}{3}\tau_3 \\ &= -\frac{1}{3}\tau_3 - \frac{1}{3}\tau_3 + \frac{2}{3}\tau_3 = 0.\end{aligned}\quad (\text{C14})$$

In the case of the forward current, the isospin sum of the exchange matrix element of the $(1 \leftrightarrow 2)$ term is

$$\begin{aligned}\sum_{t_k} \langle pk | U_F(2,1) | kh \rangle &= \sum_{t_k} \sqrt{\frac{3}{2}} \langle pk | \sum_i T_i^{(2)} T_3^{(2)\dagger} \tau_i^{(1)} | kh \rangle \\ &= \sqrt{\frac{3}{2}} \sum_{t_k} \sum_i \langle p | \tau_i | k \rangle \langle k | T_i T_3^\dagger | h \rangle = \\ &= \sqrt{\frac{3}{2}} \sum_i \langle p | \tau_i T_i T_3^\dagger | h \rangle = 0.\end{aligned}\quad (\text{C15})$$

This demonstrates the result for the forward term, that diagram (e) of Fig. 2 is zero. Analogously, the same

steps can be applied to show the result that diagram (f) for the backward term is zero. First we have

$$\begin{aligned}\sum_i T_3 T_i^\dagger \tau_i &= T_3 T_1^\dagger \tau_1 + T_3 T_2^\dagger \tau_2 + T_3 T_3^\dagger \tau_3 \\ &= -\frac{i}{3}\tau_2\tau_1 + \frac{i}{3}\tau_1\tau_2 + \frac{2}{3}\tau_3 \\ &= -\frac{1}{3}\tau_3 - \frac{1}{3}\tau_3 + \frac{2}{3}\tau_3 = 0.\end{aligned}\quad (\text{C16})$$

Then diagram (f) contain the isospin operator $U_B(1,2)$ and the isospin sum of the exchange matrix element is

$$\begin{aligned}\sum_{t_k} \langle pk | U_B(1,2) | kh \rangle &= \sum_{t_k} \sqrt{\frac{3}{2}} \langle pk | \sum_i T_3^{(1)} T_i^{(1)\dagger} \tau_i^{(2)} | kh \rangle \\ &= \sqrt{\frac{3}{2}} \sum_{t_k} \sum_i \langle p | T_3 T_i^\dagger | k \rangle \langle k | \tau_i | h \rangle \\ &= \sqrt{\frac{3}{2}} \sum_i \langle p | T_3 T_i^\dagger \tau_i | h \rangle = 0.\end{aligned}\quad (\text{C17})$$

Appendix D: Spin summations in the 1p1h MEC matrix elements

Here we perform the spin summations appearing in the exchange matrix element, given by

$$\sum_{t_k s_k} \mathbf{j}_b(p, k, k, h) = \delta_{t_p t_h} 2t_h \sum_{s_k} [\mathbf{j}_1(p, k, k, h) + \mathbf{j}_2(p, k, k, h) - 2\mathbf{j}_3(p, k, k, h)].\quad (\text{D1})$$

a. Seagull current

In the case of the seagull current only the current \mathbf{j}_3 contribute, given by Eq. (52). The sum over t_k, s_k is

$$\begin{aligned}\sum_{t_k s_k} \mathbf{j}_s(p, k, k, h) &= -4t_h \delta_{t_p t_h} \sum_{s_k} \langle s_p s_k | \frac{f^2}{m_\pi^2} F_1^V \left(\frac{\mathbf{k}_1 \cdot \boldsymbol{\sigma}^{(1)}}{\mathbf{k}_1^2 + m_\pi^2} \boldsymbol{\sigma}^{(2)} - \frac{\mathbf{k}_2 \cdot \boldsymbol{\sigma}^{(2)}}{\mathbf{k}_2^2 + m_\pi^2} \boldsymbol{\sigma}^{(1)} \right) | s_k s_h \rangle \\ &= -4t_h \delta_{t_p t_h} \frac{f^2}{m_\pi^2} F_1^V \sum_{s_k} \left(\frac{\mathbf{k}_1 \cdot \boldsymbol{\sigma}_{pk}}{\mathbf{k}_1^2 + m_\pi^2} \boldsymbol{\sigma}_{kh} - \frac{\mathbf{k}_2 \cdot \boldsymbol{\sigma}_{kh}}{\mathbf{k}_2^2 + m_\pi^2} \boldsymbol{\sigma}_{pk} \right).\end{aligned}\quad (\text{D2})$$

with $\mathbf{k}_1 = \mathbf{p} - \mathbf{k}$ and $\mathbf{k}_2 = \mathbf{k} - \mathbf{h}$. The separate spin sums are

$$\sum_{s_k} (\mathbf{k}_1 \cdot \boldsymbol{\sigma}_{pk}) \boldsymbol{\sigma}_{kh} = (\mathbf{k}_1 + i\boldsymbol{\sigma} \times \mathbf{k}_1)_{ph}, \quad \sum_{s_k} (\mathbf{k}_2 \cdot \boldsymbol{\sigma}_{kh}) \boldsymbol{\sigma}_{pk} = (\mathbf{k}_2 + i\mathbf{k}_2 \times \boldsymbol{\sigma})_{ph}.\quad (\text{D3})$$

We obtain

$$\sum_{t_k s_k} \mathbf{j}_s(p, k, k, h) = -4t_h \delta_{t_p t_h} \frac{f^2}{m_\pi^2} F_1^V \langle s_p | \left(\frac{\mathbf{k}_1 + i\boldsymbol{\sigma} \times \mathbf{k}_1}{\mathbf{k}_1^2 + m_\pi^2} - \frac{\mathbf{k}_2 + i\mathbf{k}_2 \times \boldsymbol{\sigma}}{\mathbf{k}_2^2 + m_\pi^2} \right) | s_h \rangle.\quad (\text{D4})$$

b. Pionic

In the case of the pion in flight or pionic current the sum over spin-isospin reads

$$\begin{aligned} \sum_{t_k s_k} \mathbf{j}_\pi(p, k, k, h) &= -4t_h \delta_{t_p t_h} \sum_{s_k} \langle s_p s_k | \frac{f^2}{m_\pi^2} F_1^V \frac{\mathbf{k}_1 \cdot \boldsymbol{\sigma}^{(1)} \mathbf{k}_2 \cdot \boldsymbol{\sigma}^{(2)}}{\mathbf{k}_1^2 + m_\pi^2 \mathbf{k}_2^2 + m_\pi^2} (\mathbf{k}_1 - \mathbf{k}_2) | s_k s_h \rangle \\ &= -4t_h \delta_{t_p t_h} \frac{f^2}{m_\pi^2} F_1^V \sum_{s_k} \frac{\mathbf{k}_1 \cdot \boldsymbol{\sigma}_{pk} \mathbf{k}_2 \cdot \boldsymbol{\sigma}_{kh}}{\mathbf{k}_1^2 + m_\pi^2 \mathbf{k}_2^2 + m_\pi^2} (\mathbf{k}_1 - \mathbf{k}_2) \end{aligned} \quad (\text{D5})$$

with $k_1 = \mathbf{p} - \mathbf{k}$ and $\mathbf{k}_2 = \mathbf{k} - \mathbf{h}$. The sum over spin index s_k is performed using

$$\sum_{s_k} (\mathbf{k}_1 \cdot \boldsymbol{\sigma}_{ph})(\mathbf{k}_2 \cdot \boldsymbol{\sigma}_{kh}) = \mathbf{k}_1 \cdot \mathbf{k}_2 \delta_{s_p s_h} + i(\mathbf{k}_1 \times \mathbf{k}_2) \cdot \boldsymbol{\sigma}_{ph}. \quad (\text{D6})$$

c. Δ current

From the non-relativistic Eq. (77) we can identify the three contributions, \mathbf{j}_i , to the Δ current

$$\begin{aligned} \sum_{t_k s_k} \mathbf{j}_\Delta(p, k, k, h) &= -i \delta_{t_p t_h} 2t_h C_\Delta \mathbf{q} \times \sum_{s_k} \langle s_p s_k | \frac{\mathbf{k}_1 \cdot \boldsymbol{\sigma}^{(1)}}{\mathbf{k}_1^2 + m_\pi^2} 4\mathbf{k}_1 + \frac{\mathbf{k}_2 \cdot \boldsymbol{\sigma}^{(2)}}{\mathbf{k}_2^2 + m_\pi^2} 4\mathbf{k}_2 \\ &\quad + 2i \frac{\mathbf{k}_2 \cdot \boldsymbol{\sigma}^{(2)}}{\mathbf{k}_2^2 + m_\pi^2} (\mathbf{k}_2 \times \boldsymbol{\sigma}^{(1)}) - 2i \frac{\mathbf{k}_1 \cdot \boldsymbol{\sigma}^{(1)}}{\mathbf{k}_1^2 + m_\pi^2} (\mathbf{k}_1 \times \boldsymbol{\sigma}^{(2)}) | s_k s_h \rangle \end{aligned} \quad (\text{D7})$$

with $\mathbf{k}_1 = \mathbf{p} - \mathbf{k}$ and $\mathbf{k}_2 = \mathbf{k} - \mathbf{h}$. Writing explicitly the spin indices in the Pauli matrices we have

$$\begin{aligned} \sum_{t_k s_k} \mathbf{j}_\Delta(p, k, k, h) &= -i \delta_{t_p t_h} 2t_h C_\Delta \mathbf{q} \times \sum_{s_k} \left\{ \frac{\mathbf{k}_1 \cdot \boldsymbol{\sigma}_{pk}}{\mathbf{k}_1^2 + m_\pi^2} 4\mathbf{k}_1 \delta_{s_k s_h} + \frac{\mathbf{k}_2 \cdot \boldsymbol{\sigma}_{kh}}{\mathbf{k}_2^2 + m_\pi^2} 4\mathbf{k}_2 \delta_{s_p s_k} \right. \\ &\quad \left. + 2i \frac{\mathbf{k}_2 \cdot \boldsymbol{\sigma}_{kh}}{\mathbf{k}_2^2 + m_\pi^2} (\mathbf{k}_2 \times \boldsymbol{\sigma}_{pk}) - 2i \frac{\mathbf{k}_1 \cdot \boldsymbol{\sigma}_{pk}}{\mathbf{k}_1^2 + m_\pi^2} (\mathbf{k}_1 \times \boldsymbol{\sigma}_{kh}) \right\} \end{aligned} \quad (\text{D8})$$

with $\mathbf{k}_1 = \mathbf{p} - \mathbf{k}$, and $\mathbf{k}_2 = \mathbf{k} - \mathbf{h}$. We need the following spin sums

$$\begin{aligned} \sum_{s_k} (\boldsymbol{\sigma}_{kh} \cdot \mathbf{k}_2)(\mathbf{k}_2 \times \boldsymbol{\sigma}_{pk}) &= -i [k_2^2 \boldsymbol{\sigma}_{ph} - (\boldsymbol{\sigma}_{ph} \cdot \mathbf{k}_2) \mathbf{k}_2] \\ \sum_{s_k} (\boldsymbol{\sigma}_{pk} \cdot \mathbf{k}_1)(\mathbf{k}_1 \times \boldsymbol{\sigma}_{kh}) &= i [k_1^2 \boldsymbol{\sigma}_{ph} - (\boldsymbol{\sigma}_{ph} \cdot \mathbf{k}_1) \mathbf{k}_1]. \end{aligned} \quad (\text{D9})$$

The result for the sum over s_k is

$$\sum_{t_k s_k} \mathbf{j}_\Delta(p, k, k, h) = -4it_h \delta_{t_p t_h} C_\Delta \mathbf{q} \times \left\{ \frac{k_1^2 \boldsymbol{\sigma}_{ph} + (\boldsymbol{\sigma}_{ph} \cdot \mathbf{k}_1) \mathbf{k}_1}{k_1^2 + m_\pi^2} + \frac{k_2^2 \boldsymbol{\sigma}_{ph} + (\boldsymbol{\sigma}_{ph} \cdot \mathbf{k}_2) \mathbf{k}_2}{k_2^2 + m_\pi^2} \right\} \quad (\text{D10})$$

Appendix E: Spin summations in the interference responses

Here we compute the spin summations in the 1b2b interference response function.

In this appendix we use the notation $\mathbf{k}_1 = \mathbf{p} - \mathbf{k}$ and $\mathbf{k}_2 = \mathbf{k} - \mathbf{h}$. We use also the identities $\mathbf{k}_1 + \mathbf{k}_2 = \mathbf{q}$, and $\mathbf{k}_1 = \mathbf{q} - \mathbf{k}_2$.

a. Magnetization-seagull

Inserting Eq. (86) into Eq. (90) we have

$$w_{ms}^T = 4t_h \delta_{t_p t_h} \frac{G_M^h f^2}{2m_N m_\pi^2} F_1^V \int \frac{d^3 k}{(2\pi)^3} \sum_{s_p s_h} i(\mathbf{q} \times \boldsymbol{\sigma}_{hp}) \cdot \left(\frac{\delta_{s_p s_h} \mathbf{k}_1 + i\boldsymbol{\sigma}_{ph} \times \mathbf{k}_1}{\mathbf{k}_1^2 + m_\pi^2} - \frac{\delta_{s_p s_h} \mathbf{k}_2 + i\mathbf{k}_2 \times \boldsymbol{\sigma}_{ph}}{\mathbf{k}_2^2 + m_\pi^2} \right). \quad (\text{E1})$$

The sums involved inside the integral are of the kind:

$$\sum_{s_p s_h} i(\mathbf{q} \times \boldsymbol{\sigma}_{hp}) \cdot \delta_{s_p s_h} \mathbf{k} = \sum_{s_h} i(\mathbf{q} \times \boldsymbol{\sigma}_{hh}) \cdot \mathbf{k} = 0 \quad (\text{E2})$$

$$\begin{aligned} \sum_{s_p s_h} i(\mathbf{q} \times \boldsymbol{\sigma}_{hp}) \cdot (i\boldsymbol{\sigma}_{ph} \times \mathbf{k}) &= - \sum_{s_p s_h} (\mathbf{q} \cdot \boldsymbol{\sigma}_{ph} \boldsymbol{\sigma}_{hp} \cdot \mathbf{k} - \mathbf{q} \cdot \mathbf{k} \boldsymbol{\sigma}_{hp} \cdot \boldsymbol{\sigma}_{ph}) = -\text{Tr}(q^i \sigma_i \sigma_j k^j - \mathbf{q} \cdot \mathbf{k} \sigma_i \sigma_i) \\ &= -\text{Tr}(q^i \delta_{ij} k^j - 3\mathbf{q} \cdot \mathbf{k}) = 4\mathbf{q} \cdot \mathbf{k}. \end{aligned} \quad (\text{E3})$$

Therefore

$$w_{ms}^T = 4t_h \delta_{t_p t_h} \frac{G_M^h f^2}{2m_N m_\pi^2} F_1^V \int \frac{d^3 k}{(2\pi)^3} \left(\frac{4\mathbf{q} \cdot \mathbf{k}_1}{\mathbf{k}_1^2 + m_\pi^2} + \frac{4\mathbf{q} \cdot \mathbf{k}_2}{\mathbf{k}_2^2 + m_\pi^2} \right). \quad (\text{E4})$$

b. Convection-seagull

Inserting Eq. (86) into Eq. (91) we have

$$\begin{aligned} w_{cs}^T &= 4t_h \delta_{t_p t_h} \frac{G_E^h f^2}{m_N m_\pi^2} F_1^V \int \frac{d^3 k}{(2\pi)^3} \sum_{s_p s_h} \delta_{s_h s_p} \mathbf{h}_T \cdot \left(\frac{\delta_{s_p s_h} \mathbf{k}_1 + i\boldsymbol{\sigma}_{ph} \times \mathbf{k}_1}{\mathbf{k}_1^2 + m_\pi^2} - \frac{\delta_{s_p s_h} \mathbf{k}_2 + i\mathbf{k}_2 \times \boldsymbol{\sigma}_{ph}}{\mathbf{k}_2^2 + m_\pi^2} \right). \\ &= 4t_h \delta_{t_p t_h} \frac{G_E^h f^2}{m_N m_\pi^2} F_1^V \int \frac{d^3 k}{(2\pi)^3} \left(\frac{\mathbf{h}_T \cdot \mathbf{k}_1}{\mathbf{k}_1^2 + m_\pi^2} - \frac{\mathbf{h}_T \cdot \mathbf{k}_2}{\mathbf{k}_2^2 + m_\pi^2} \right). \end{aligned} \quad (\text{E5})$$

c. Magnetization-pionic

Inserting Eq. (87) into Eq. (92) we have

$$w_{m\pi}^T = 4t_h \delta_{t_p t_h} \frac{G_M^h f^2}{2m_N m_\pi^2} F_1^V \int \frac{d^3 k}{(2\pi)^3} \sum_{s_p s_h} i(\mathbf{q} \times \boldsymbol{\sigma}_{hp}) \cdot (\mathbf{k}_1 - \mathbf{k}_2) \frac{\delta_{s_p s_h} \mathbf{k}_1 \cdot \mathbf{k}_2 + i(\mathbf{k}_1 \times \mathbf{k}_2) \cdot \boldsymbol{\sigma}_{ph}}{(\mathbf{k}_1^2 + m_\pi^2)(\mathbf{k}_2^2 + m_\pi^2)}. \quad (\text{E6})$$

The sum over spin inside the integral is

$$\begin{aligned} \sum_{s_p s_h} i(\mathbf{q} \times \boldsymbol{\sigma}_{hp}) \cdot (\mathbf{k}_1 - \mathbf{k}_2) [\delta_{s_p s_h} \mathbf{k}_1 \cdot \mathbf{k}_2 + i(\mathbf{k}_1 \times \mathbf{k}_2) \cdot \boldsymbol{\sigma}_{ph}] &= - \sum_{s_p s_h} (\mathbf{q} \times \boldsymbol{\sigma}_{hp}) \cdot (\mathbf{k}_1 - \mathbf{k}_2) (\mathbf{k}_1 \times \mathbf{k}_2) \cdot \boldsymbol{\sigma}_{ph} \\ &= - \sum_{s_p s_h} [(\mathbf{k}_1 - \mathbf{k}_2) \times \mathbf{q}] \cdot \boldsymbol{\sigma}_{hp} (\mathbf{k}_1 \times \mathbf{k}_2) \cdot \boldsymbol{\sigma}_{ph} = -2[(\mathbf{k}_1 - \mathbf{k}_2) \times \mathbf{q}] \cdot (\mathbf{k}_1 \times \mathbf{k}_2) \\ &= -4(\mathbf{q} \times \mathbf{k}_2)^2 \end{aligned} \quad (\text{E7})$$

where we have used that

$$\sum_{s_p s_h} (\mathbf{a} \cdot \boldsymbol{\sigma}_{hp}) (\mathbf{b} \cdot \boldsymbol{\sigma}_{ph}) = \text{Tr}(a^i \sigma_i \sigma_j b^j) = 2\mathbf{a} \cdot \mathbf{b} \quad (\text{E8})$$

$$\mathbf{k}_1 = \mathbf{q} - \mathbf{k}_2 \quad (\text{E9})$$

$$(\mathbf{k}_1 - \mathbf{k}_2) \times \mathbf{q} = (\mathbf{q} - 2\mathbf{k}_2) \times \mathbf{q} = 2\mathbf{q} \times \mathbf{k}_2 \quad (\text{E10})$$

$$\mathbf{k}_1 \times \mathbf{k}_2 = (\mathbf{q} - \mathbf{k}_2) \times \mathbf{k}_2 = \mathbf{q} \times \mathbf{k}_2. \quad (\text{E11})$$

With the result of Eq. (E7), we obtain

$$w_{m\pi}^T = 4t_h \delta_{t_p t_h} \frac{G_M^h f^2}{2m_N m_\pi^2} F_1^V \int \frac{d^3 k}{(2\pi)^3} \frac{-4(\mathbf{q} \times \mathbf{k}_2)^2}{(\mathbf{k}_1^2 + m_\pi^2)(\mathbf{k}_2^2 + m_\pi^2)}. \quad (\text{E12})$$

d. Convection-pionic

Inserting Eq. (87) into Eq. (93) we have

$$w_{c\pi}^T = 4t_h \delta_{t_p t_h} \frac{G_E^h}{m_N} \frac{f^2}{m_\pi^2} F_1^V \int \frac{d^3 k}{(2\pi)^3} \sum_{s_p s_h} \delta_{s_h s_p} \mathbf{h}_T \cdot (\mathbf{k}_1 - \mathbf{k}_2) \frac{\delta_{s_p s_h} \mathbf{k}_1 \cdot \mathbf{k}_2 + i(\mathbf{k}_1 \times \mathbf{k}_2) \cdot \boldsymbol{\sigma}_{ph}}{(\mathbf{k}_1^2 + m_\pi^2)(\mathbf{k}_1^2 + m_\pi^2)}. \quad (\text{E13})$$

Sum over spin inside the integral:

$$\begin{aligned} \sum_{s_p s_h} \delta_{s_h s_p} \mathbf{h}_T \cdot (\mathbf{k}_1 - \mathbf{k}_2) [\delta_{s_p s_h} \mathbf{k}_1 \cdot \mathbf{k}_2 + i(\mathbf{k}_1 \times \mathbf{k}_2) \cdot \boldsymbol{\sigma}_{ph}] &= \sum_{s_h} \mathbf{h}_T \cdot (\mathbf{k}_1 - \mathbf{k}_2) (\mathbf{k}_1 \cdot \mathbf{k}_2) \\ &= 2\mathbf{h}_T \cdot (\mathbf{q} - 2\mathbf{k}_2) [(\mathbf{q} - \mathbf{k}_2) \cdot \mathbf{k}_2] = -4(\mathbf{h}_T \cdot \mathbf{k}_2)(\mathbf{q} \cdot \mathbf{k}_2 - \mathbf{k}_2^2). \end{aligned} \quad (\text{E14})$$

Then we obtain

$$w_{c\pi}^T = 4t_h \delta_{t_p t_h} \frac{G_E^h}{m_N} \frac{f^2}{m_\pi^2} F_1^V \int \frac{d^3 k}{(2\pi)^3} \frac{-4(\mathbf{h}_T \cdot \mathbf{k}_2)(\mathbf{q} \cdot \mathbf{k}_2 - \mathbf{k}_2^2)}{(\mathbf{k}_1^2 + m_\pi^2)(\mathbf{k}_1^2 + m_\pi^2)}. \quad (\text{E15})$$

e. Magnetization- Δ

Inserting Eq. (88) into Eq. (94) we have

$$w_{m\Delta}^T = 4t_h \delta_{t_p t_h} \frac{G_M^h}{2m_N} C_\Delta \int \frac{d^3 k}{(2\pi)^3} \sum_{s_p s_h} i(\mathbf{q} \times \boldsymbol{\sigma}_{hp}) \cdot \left[i\mathbf{q} \times \left(\frac{\mathbf{k}_1^2 \boldsymbol{\sigma}_{ph} + (\boldsymbol{\sigma}_{ph} \cdot \mathbf{k}_1) \mathbf{k}_1}{\mathbf{k}_1^2 + m_\pi^2} + \frac{\mathbf{k}_2^2 \boldsymbol{\sigma}_{ph} + (\boldsymbol{\sigma}_{ph} \cdot \mathbf{k}_2) \mathbf{k}_2}{\mathbf{k}_2^2 + m_\pi^2} \right) \right]. \quad (\text{E16})$$

We need the following spin sums. The first one is similar to Eq. (E3)

$$\sum_{s_p s_h} (\mathbf{q} \times \boldsymbol{\sigma}_{hp}) \cdot (\mathbf{q} \times \boldsymbol{\sigma}_{ph}) = 4q^2. \quad (\text{E17})$$

The second sum required is

$$\begin{aligned} \sum_{s_p s_h} (\mathbf{q} \times \boldsymbol{\sigma}_{hp}) \cdot (\mathbf{q} \times \mathbf{k}_1) (\boldsymbol{\sigma}_{ph} \cdot \mathbf{k}_1) &= \sum_{s_p s_h} [q^2 \boldsymbol{\sigma}_{hp} \cdot \mathbf{k}_1 - (\mathbf{q} \cdot \mathbf{k}_1)(\mathbf{q} \cdot \boldsymbol{\sigma}_{hp})] (\boldsymbol{\sigma}_{ph} \cdot \mathbf{k}_1) \\ &= q^2 \sum_{s_p s_h} (\boldsymbol{\sigma}_{hp} \cdot \mathbf{k}_1) (\boldsymbol{\sigma}_{ph} \cdot \mathbf{k}_1) - (\mathbf{q} \cdot \mathbf{k}_1) \sum_{s_p s_h} (\mathbf{q} \cdot \boldsymbol{\sigma}_{hp}) (\boldsymbol{\sigma}_{ph} \cdot \mathbf{k}_1) \\ &= 2q^2 k_1^2 - 2(\mathbf{q} \cdot \mathbf{k}_1)^2 \end{aligned} \quad (\text{E18})$$

where we have used twice Eq. (E8). Using these results the $m\Delta$ response function is

$$w_{m\Delta}^T = -4t_h \delta_{t_p t_h} \frac{G_M^h}{2m_N} C_\Delta \int \frac{d^3 k}{(2\pi)^3} \left(\frac{6q^2 k_1^2 - 2(\mathbf{q} \cdot \mathbf{k}_1)^2}{\mathbf{k}_1^2 + m_\pi^2} + \frac{6q^2 k_2^2 - 2(\mathbf{q} \cdot \mathbf{k}_2)^2}{\mathbf{k}_2^2 + m_\pi^2} \right). \quad (\text{E19})$$

Appendix F: Spectral function and hadronic tensor

The spectral function is obtained by assuming plane waves for the final nucleon. This assumption leads to a factorization approximation for the response function within the impulse approximation, where the current is considered to be one-body only. In this framework, the response function can be factored into a product of the current matrix element and the spectral function, which

describes the distribution of hole states in the nucleus.

We assume that the initial nuclear state is a spin-zero nucleus at rest with energy $E_i = M_A$, and wave function:

$$|i\rangle = |\Phi_0^{(A)}\rangle. \quad (\text{F1})$$

The final state correspond to a plane wave particle and a residual $A - 1$ nucleus

$$|f\rangle = |\Phi_\alpha^{(A-1)}, \mathbf{p}, s\rangle = a_{\mathbf{p},s}^\dagger |\Phi_\alpha^{(A-1)}\rangle. \quad (\text{F2})$$

The label α denotes the quantum numbers of the daughter nucleus in an excited state with excitation energy $\epsilon_\alpha^{(A-1)}$. Then the final energy, neglecting the recoil energy is,

$$E_f = m_N + T_p + M_{A-1} + \epsilon_\alpha^{(A-1)} \quad (\text{F3})$$

where $T_p = p^2/2m_N$. Then the diagonal component of the hadronic tensor is,

$$W^{\mu\mu} = \sum_{\alpha\mathbf{p}\mathbf{s}} |\langle \Phi_\alpha^{(A-1)}, \mathbf{p}, s | J^\mu(\mathbf{q}) | \Phi_0^{(A)} \rangle|^2 \delta(E_i + \omega - E_f). \quad (\text{F4})$$

Assuming that the current is a one-body operator and ignoring the final nucleon spin for simplicity we have,

$$W^{\mu\mu} = \sum_{\alpha\mathbf{p}} |\langle \Phi_\alpha^{(A-1)} | a_{\mathbf{p}} \int d^3k J^\mu(\mathbf{q} + \mathbf{k}, \mathbf{k}) a_{\mathbf{q}+\mathbf{k}}^\dagger a_{\mathbf{k}} | \Phi_0^{(A)} \rangle|^2 \delta(M_A + \omega - m_N - T_p - M_{A-1} - \epsilon_\alpha^{(A-1)}). \quad (\text{F5})$$

Using the commutation properties of the creation and annihilation operators,

$$a_{\mathbf{p}} a_{\mathbf{q}+\mathbf{k}}^\dagger = \delta(\mathbf{p} - \mathbf{q} - \mathbf{k}) - a_{\mathbf{q}+\mathbf{k}}^\dagger a_{\mathbf{p}}, \quad (\text{F6})$$

and assuming that the final particle momentum is large enough to neglect high-momentum components in the initial wave function (as the dominant contribution comes from momenta below the Fermi momentum), $a_{\mathbf{p}} | \Phi_0^{(A)} \rangle \simeq 0$, then the hadronic tensor is

$$W^{\mu\mu} = \sum_{\alpha} \int d^3p |\langle \Phi_\alpha^{(A-1)} | J^\mu(\mathbf{p}, \mathbf{p} - \mathbf{q}) a_{\mathbf{p}-\mathbf{q}} | \Phi_0^{(A)} \rangle|^2 \delta(M_A + \omega - m_N - T_p - M_{A-1} - \epsilon_\alpha^{(A-1)}). \quad (\text{F7})$$

Introducing the separation energy $S = M_{A-1} + m_N - M_A > 0$ and the missing energy $E_m = \omega - T_p$ then

$$W^{\mu\mu} = \int d^3p |J^\mu(\mathbf{p}, \mathbf{p} - \mathbf{q})|^2 S(\mathbf{p} - \mathbf{q}, E_m)$$

where the one-hole spectral function is defined as,

$$S(\mathbf{h}, E) = \sum_{\alpha, s} |\langle \Phi_\alpha^{(A-1)} | a_{\mathbf{h}, s} | \Phi_0^{(A)} \rangle|^2 \delta(E - S - \epsilon_\alpha^{(A-1)}).$$

-
- [1] R. Cenni, *Electromagnetic Response Functions of Nuclei*, Nova Science Publishers, Inc. (Huntington, New York) 2001.
- [2] S. Boffi, C. Giusti, F.D. Pacati, and M. Radici. *Electromagnetic Response of Atomic Nuclei*, Oxford University Press (New York) 1996.
- [3] E. J. Moniz, I. Sick, R. R. Whitney, J. R. Ficenec, R. D. Kephart, and W. P. Trower, Phys. Rev. Lett. 26 (1971) 445.
- [4] R. R. Whitney, I. Sick, J. R. Ficenec, R. D. Kephart, and W. P. Trower, Phys. Rev. C 9 (1974) 2230.
- [5] R. Rosenfelder, Ann. Phys. (N.Y.) 128, 188 (1980).
- [6] C.J. Horowitz and J. Piekarewicz, Nuclear Physics A 511 (1990) 461.
- [7] K. Wehrberger, Phys. Rep. 225 (1993) 273.
- [8] A.M. Saruis, Phys. Rep. 235 (1993) 57.
- [9] J. Jourdan, Nucl. Phys. A 603 (1996) 117.
- [10] J. Carlson, J. Jourdan, R. Schiavilla, and I. Sick, Phys. Rev. C 65 (2002) 024002.
- [11] L. Alvarez-Ruso, Y. Hayato, J. Nieves, New J. Phys. 16 (2014) 075015.
- [12] U. Mosel, Ann. Rev. Nuc. Part. Sci. 66 (2016), 171.
- [13] T. Katori and M. Martini, J. Phys. G 45 (2018) no.1, 013001.
- [14] A. M. Ankowski, C. Mariani, J. Phys. G44 (2017) 054001.
- [15] O. Benhar, P. Huber, C. Mariani, D. Meloni, Phys. Rep. 700 (2017) 1.
- [16] L. Alvarez-Ruso *et al.* [NuSTEC], Prog. Part. Nucl. Phys. 100, 1-68 (2018).
- [17] J. E. Amaro, M. B. Barbaro, J. A. Caballero, R. González-Jiménez, G. D. Megias and I. Ruiz Simo, J. Phys. G 47 (2020) no.12, 124001.
- [18] A. M. Ankowski, A. Ashkenazi, S. Bacca, J. L. Barrow, M. Betancourt, A. Bodek, M. E. Christy, L. D. S. Dytman, A. Friedland and O. Hen, *et al.* J. Phys. G 50, no.12, 120501 (2023).
- [19] L. A. Ruso, A. M. Ankowski, S. Bacca, A. B. Balantekin, J. Carlson, S. Gardiner, R. González-Jiménez, R. Gupta, T. J. Hobbs and M. Hoferichter, *et al.* J. Phys. G (2025) in press, doi:10.1088/1361-6471/adae26 [arXiv:2203.09030 [hep-ph]].
- [20] P. E. Bosted and V. Mamyan, [arXiv:1203.2262 [nucl-th]].
- [21] A. Bodek and M. E. Christy, Phys. Rev. C 106, no.6, L061305 (2022).
- [22] A. Lovato, S. Gandolfi, J. Carlson, S. C. Pieper and R. Schiavilla, Phys. Rev. Lett. 117, no.8, 082501 (2016).
- [23] J. W. Van Orden and T. W. Donnelly, Annals Phys. 131, 451-493 (1981).
- [24] W. Alberico, M. Ericson, and A. Molinari, Ann. Phys. (N.Y.) 154 (1984) 356.
- [25] M. J. Dekker, P. J. Brussaard and J. A. Tjon, Phys. Rev. C 49, 2650-2670 (1994).
- [26] A. De Pace, M. Nardi, W. M. Alberico, T. W. Donnelly and A. Molinari, Nucl. Phys. A 726, 303-326 (2003).
- [27] M. Martini, M. Ericson, G. Chanfray, J. Marteau, Phys.Rev. C80 (2009) 065501.
- [28] M. Martini, M. Ericson and G. Chanfray, Phys. Rev. C 84, 055502 (2011).
- [29] J. Nieves, I. Ruiz Simo, M.J. Vicente Vacas, Phys.Rev. C83 (2011) 045501.
- [30] G. D. Megias, T. W. Donnelly, O. Moreno, C. F. Williamson, J. A. Caballero, R. González-Jiménez, A. De Pace, M. B. Barbaro, W. M. Alberico and M. Nardi, *et al.* Phys. Rev. D 91, no.7, 073004

- (2015).
- [31] G. D. Megias, J. E. Amaro, M. B. Barbaro, J. A. Caballero and T. W. Donnelly, *Phys. Rev. D* **94**, 013012 (2016).
- [32] T. Van Cuyck, N. Jachowicz, R. González-Jiménez, J. Ryckebusch and N. Van Dessel, *Phys. Rev. C* **95**, no.5, 054611 (2017).
- [33] J.E. Amaro, M.B. Barbaro, J.A. Caballero, T.W. Donnelly, and A. Molinari, *Nucl. Phys. A* **643** (1998) 349.
- [34] J.E. Amaro, M.B. Barbaro, J.A. Caballero, T.W. Donnelly, and A. Molinari, *Nucl. Phys. A* **697** (2002) 388.
- [35] J. E. Amaro, M. B. Barbaro, J. A. Caballero, T. W. Donnelly and A. Molinari, *Phys. Rept.* **368**, 317-407 (2002).
- [36] M. Kohno and N. Ohtsuka, *Phys. Lett. B* **98**, 335-339 (1981).
- [37] W. M. Alberico, T. W. Donnelly and A. Molinari, *Nucl. Phys. A* **512**, 541-590 (1990).
- [38] J. E. Amaro, A. M. Lallena and G. Co, *Int. Jou. Mod. Phys E* **3** (1994), 735.
- [39] J. E. Amaro, A. M. Lallena and G. Co, *Nucl. Phys. A* **578**, 365-396 (1994).
- [40] J. E. Amaro, M. B. Barbaro, J. A. Caballero, T. W. Donnelly and A. Molinari, *Nucl. Phys. A* **723**, 181-204 (2003).
- [41] P. R. Casale, J. E. Amaro and M. B. Barbaro, *Symmetry* **15**, no.9, 1709 (2023).
- [42] A. Fabrocini, *Phys. Rev. C* **55**, 338-348 (1997).
- [43] W. Leidemann and G. Orlandini, *Nucl. Phys. A* **506**, 447-470 (1990).
- [44] A. Lovato, S. Gandolfi, J. Carlson, S. C. Pieper and R. Schiavilla, *Phys. Rev. Lett.* **112**, no.18, 182502 (2014).
- [45] T. Franco-Munoz, J. García-Marcos, R. González-Jiménez and J. M. Udías, *Phys. Rev. C* **108**, no.6, 064608 (2023).
- [46] T. Franco-Munoz, R. González-Jiménez and J. M. Udías, *J. Phys. G* **52** (2025) no.2, 025103.
- [47] A. Lovato, N. Rocco and N. Steinberg, [arXiv:2312.12545 [nucl-th]].
- [48] D.O. Riska, *Phys. Rep.* **181** (1989) 207.
- [49] R. Schiavilla, V. R. Pandharipande and D. O. Riska, *Phys. Rev. C* **40**, 2294-2309 (1989).
- [50] S. Frullani and J Mougey, in *Ad. Nucl. Phys.* vol. 14. Plenum Press (New York) 1984.
- [51] T. Ericson, W. Weise, *Pions and Nuclei*, Oxford University Press (New York), 1988.
- [52] D.O. Riska, in *Mesons in Nuclei*, Eds. M. Rho and D.H. Wilkinson, North-Holland Publishing Company (Amsterdam), 1979.
- [53] I. Ruiz Simo, J. E. Amaro, M. B. Barbaro, A. De Pace, J. A. Caballero and T. W. Donnelly, *J. Phys. G* **44**, no.6, 065105 (2017).
- [54] E. Hernandez, J. Nieves and M. Valverde, *Phys. Rev. D* **76** (2007), 033005.
- [55] S. Dolan, G. D. Megias and S. Bolognesi, *Phys. Rev. D* **101** (2020) no.3, 033003.
- [56] V. Pascalutsa, O. Scholten, *Nucl. Phys. A* **591** (1995), 658.
- [57] B. Sommer, *Nucl. Phys. A* **308**, 263-289 (1978).
- [58] R. Machleidt, K. Holinde, and Ch. Elster, *Phys. Rep.* **149** (1987) 1.
- [59] C.H. Llewellyn Smith, *Phys. Rep.* **5** (1972) 261.
- [60] J. M. Udias, P. Sarriguren, E. Moya de Guerra, E. Garrido and J. A. Caballero, *Phys. Rev. C* **51**, 3246-3255 (1995).
- [61] C.J Horowitz, D.P. Murdock, B.D Serot, in *Computational Nuclear Physics 1*, K. Langanke, J.A. Maruhn and S.E. Koonin (Eds.), Springer Verlag (1991), Berlin.
- [62] V. L. Martinez-Consentino, I. R. Simo and J. E. Amaro, *Phys. Rev. C* **104**, no.2, 025501 (2021).
- [63] J. E. Amaro, M. B. Barbaro, J. A. Caballero, T. W. Donnelly, A. Molinari and I. Sick, *Phys. Rev. C* **71**, 015501 (2005).
- [64] P. R. Casale, J. E. Amaro, V. L. Martinez-Consentino and I. Ruiz Simo, *Universe* **9**, no.4, 158 (2023).
- [65] J. E. Amaro, M. B. Barbaro, J. A. Caballero, T. W. Donnelly, C. Maieron and J. M. Udias, *Phys. Rev. C* **81**, 014606 (2010).
- [66] J. E. Amaro, M. B. Barbaro, J. A. Caballero, T. W. Donnelly and C. Maieron, *Phys. Rev. C* **71**, 065501 (2005).
- [67] O. Benhar, A. Fabrocini, S. Fantoni and I. Sick, *Nucl. Phys. A* **579** (1994), 493-517.
- [68] S. Boffi, C. Giusti, F. D. Pacati and M. Radici, *Nucl. Phys. A* **518** (1990), 639-657.
- [69] P. R. Casale, J. E. Amaro, E. Ruiz Arriola and I. Ruiz Simo, *Phys. Rev. C* **108** (2023) no.5, 054001.